Synthesis and Luminescence of Cyclometalated Compounds with Nitrile and Isocyanide Ligands†

Álvaro Díez,‡ Juan Forniés,§ Sara Fuertes,§ Elena Lalinde,*,‡ Carmen Larraz,§ José A. López,§ Antonio Martín,§ M. Teresa Moreno,‡ and Violeta Sicilia*,⊥

Departamento de Química, Grupo de Síntesis Química de La Rioja, UA-CSIC, Universidad de La Rioja, 26006, Logroño, Spain, Departamento de Química Inorgánica, Instituto de Ciencia de Materiales de Aragón, Facultad de Ciencias, Universidad de Zaragoza-CSIC, Plaza. S. Francisco s/n 50009 Zaragoza, Spain, and Departamento de Química Inorgánica, Instituto de Ciencia de Materiales de Aragón, Escuela Universitaria de Ingeniería Técnica Industrial, Universidad de Zaragoza-CSIC, Campus Universitario del Actur, Edificio Torres Quevedo, 50018, Zaragoza, Spain

Received September 1, 2008

Mononuclear cationic cyclometalated palladium complexes $[Pd(C^N)(NCMe)_2]ClO_4$ [C^N = benzoquinolinate (bzq) **1**, 2-phenylpyridinate (ppy) **2**], analogous to the previously described platinum complexes $[Pt(C^N)(NCMe)_2]ClO_4$ [C^N = bzq **3**, ppy **4**], and the isocyanide platinum benzoquinolinate $[Pt(bzq)(CNR)_2]X$ (R = *tert*-butyl (*t*-Bu, **5**), 2,6-dimethylphenyl (Xyl, **6**), 2-naphthyl (2-Np, **7**); X = ClO_4^- **a**, PF_6^- **b**) have been prepared and characterized. The solid-state structures of the cation $[Pt(C^N)(CN\text{-}Xyl)_2]^+$ with different counteranions (**6a** and **6b**) were found to be different in terms of packing, although in both cases they were dominated by $\pi-\pi$ intermolecular interactions. The influence of the counteranion in the UV−vis spectra, both in solution and in the solid state of **5**−**7**, is negligible. Time-dependent density-functional theory calculations on cation $[Pt(C^N)(CN\text{-}Xyl)_2]^+$ (**6**$^+$) have been performed, suggesting that the lowest absorption is ^{1}IL in nature mixed with some ^{1}MLCT character. Acetonitrile platinum complexes (**3**, **4**) are photoluminescent at low temperature (77 K) and at room temperature, whereas analogous palladium complexes (**1**, **2**) are emissive only at 77 K (solid-state and glassy acetonitrile). Isocyanide derivatives **5**−**7** are intensely luminescent in all media. The emissions are assigned to ligand-centered fluorescence, to mixed ^{3}LC/^{3}MLCT phosphorescence, or to excimeric (or ground-state) $^3\pi\pi^*$ or ^{3}MMLCT [$\sigma^*(M)\rightarrow\pi^*(C^N)$] transitions depending on the medium and the excitation wavelength. The effect of the counteranion in governing the degree of aggregation and the extent of the interactions seem to be relatively important, especially in a rigid medium, with the smaller ClO_4^- inducing a more excimeric character. The tendency to form $\pi-\pi$ excimers and/or Pt···Pt oligomerization follows the order CN-2-Np > CN-*t*-Bu > CN-Xyl and ClO_4^- > PF_6^-.

Introduction

Platinum cyclometalated complexes have received considerable attention in recent years because of their interesting photochemical and photophysical properties such as good stability, high photoluminescence quantum yields, short triplet-state lifetimes (several microseconds), and ease of spectral tuning.[1−25] Many of these complexes have been successfully applied as phosphorescent dopants in the fabrication of highly efficient organic light-emitting devices (OLEDs).[26−28] Compared to analogous Pt(II) luminophores, luminescent cyclopalladated complexes are rare, and with very few exceptions,[29−31] most systems emit only at low temperatures and with low

† Dedicated to Professor Antonio Laguna on the occasion of his 60th anniversary.

* Corresponding authors. E-mail: forniesj@unizar.es. Fax: (+34)976-761159. E-mail: elena.lalinde@dq.unirioja.es. Fax: (+34)941-299621. E-mail: sicilia@unizar.es. Fax: (+34)976-762189.

‡ Universidad de La Rioja, UA-CSIC.

§ Facultad de Ciencias, Universidad de Zaragoza-CSIC.

⊥ Escuela Universitaria de Ingeniería Técnica Industrial, Universidad de Zaragoza-CSIC.

(1) Williams, J. A. G. *Top. Curr. Chem.* **2007**, *281*, 205.
(2) Koo, C. K.; Ho, Y. M.; Chow, C. F.; Lam, M. H. W.; Lau, T. C.; Wong, W. Y. *Inorg. Chem.* **2007**, *46*, 3603.
(3) Yang, C.; Zhang, X.; You, H.; Zhu, L.; Chen, L.; Zhu, L.; Tao, Y.; Ma, D.; Shuai, Z.; Qin, J. *Adv. Funct. Mater.* **2007**, *17*, 651.
(4) Berenguer, J. R.; Lalinde, E.; Torroba, J. *Inorg. Chem.* **2007**, *46*, 9919.
(5) Yin, B.; Niemeyer, F.; Williams, J. A. G.; Jiang, J.; Boucekkine, A.; Toupet, L.; Le Bozec, H.; Guerchais, V. *Inorg. Chem.* **2006**, *45*, 8584.
(6) Kui, S. C. F.; Chui, S. S. Y.; Che, C. M.; Zhu, N. *J. Am. Chem. Soc.* **2006**, *128*, 8297.
(7) He, Z.; Wong, W. Y.; Yu, X.; Kwok, H. S.; Lin, Z. *Inorg. Chem.* **2006**, *45*, 10922.
(8) Wong, W. Y.; He, Z.; So, S. K.; Tong, K. L.; Lin, Z. *Organometallics* **2005**, *24*, 4079.
(9) Thomas III, S. W.; Venkatesan, K.; Müller, P.; Swager, T. M. *J. Am. Chem. Soc.* **2006**, *128*, 16641.
(10) Shavaleev, N. M.; Adams, H.; Best, J.; Edge, R.; Navaratnam, S.; Weinstein, J. A. *Inorg. Chem.* **2006**, *45*, 9410.
(11) Sun, W.; Zhu, H.; Barron, P. M. *Chem. Mater.* **2006**, *18*, 2602.
(12) Jude, H.; Krause Bauer, J. A.; Connick, W. B. *Inorg. Chem.* **2005**, *44*, 1211.
(13) Ionkin, A. S.; Marshall, W. J.; Wang, Y. *Organometallics* **2005**, *24*, 619.
(14) Ma, B.; Li, J.; Djurovich, P. I.; Yousufuddin, M.; Bau, R.; Thompson, M. E. *J. Am. Chem. Soc.* **2005**, *127*, 28.
(15) Laskar, I. R.; Hsu, S. F.; Chen, T. M. *Polyhedron* **2005**, *24*, 881.
(16) Farley, S. J.; Rochester, D. L.; Thompson, A. L.; Howard, J. A. K.; Williams, J. A. G. *Inorg. Chem.* **2005**, *44*, 9690.
(17) Díez, A.; Forniés, J.; García, A.; Lalinde, E.; Moreno, M. T. *Inorg. Chem.* **2005**, *44*, 2443.
(18) Jolliet, P.; Gianini, M.; von Zelewsky, A.; Bernardinelli, G.; Stoeckli-Evans, H. *Inorg. Chem.* **1996**, *35*, 4883.
(19) DePriest, J.; Zheng, G. Y.; Woods, C.; Rillema, D. P.; Mikirova, N. A.; Zandler, M. E. *Inorg. Chim. Acta* **1997**, *264*, 287.

10.1021/om800845c CCC: $40.75
Publication on Web 02/17/2009

efficiency.[32−38] Emission of isolated Pt(II) cyclometalated complexes is typically assigned to ligand-centered (LC) and/or metal-to-ligand charge transfer (MLCT) states. In addition, the square-planar structure of Pt(II) complexes gives rise to the possibility of ground- and excited-state interactions including aggregation and excimer or exciplex formation,[4,6,13,15,16,39] depending on the concentration and proximity of the molecules, leading to marked red shifts relative to the mononuclear emission spectra. These transitions are assigned to metal−metal-to-ligand charge transfer (MLCT) or excimeric ligand-to-ligand charge transfer. In addition, some investigations have shown that the color and emissive properties of crystalline Pt(II) bipyridyl, terpyridyl, or cyclometalated salts are highly dependent upon the chosen counterion for crystallization,[40−45] and differences in the extent of $\pi-\pi$ and/or Pt···Pt interactions are usually invoked to explain the phenomena.

Thus, photoluminescence-tuning Pt(II) complexes from near-UV to deep red have been reported. There are two alternatives for tuning emission in isolated complexes: modification of the cyclometalating ring system or variation of the ancillary ligands. Our research group has used both methodologies. We have reported efficient color tuning by employing heteroleptic Pt(II) complexes with one bidentate cyclometalating ligand (benzoquinolinate ligand) and monodentate ancillary ligands such as phosphine,[17] alkynylphosphine,[17] alkynyl,[46] or cyanide ligands[47] incorporating substituents with different electronic behavior. Furthermore, we have employed a terdentate ligand [C^N^C (HC^N^C = 2,6-diphenylpyridine)] introducing alkynyl, CN, S-2py, or CH_2COCH_3 anionic groups into the fourth site.[4]

In this report, we describe the synthesis, structure, and photophysical properties of C^N coordinated palladium and platinum complexes [C^N = benzoquinolinate (bzq), 2-phenylpyridinate (ppy)] incorporating monodentate ligands with different electron-withdrawing/donating properties. For comparative purposes, we have chosen groups isoelectronic to the previously studied anionic alkynyl ligands: a weak-field ligand as the acetonitrile (NCMe) molecule and strong-field ligands as isocyanide groups (CNR; R = *t*-Bu, Xyl, 2-Np). In recent years, several platinum(II) and palladium(II) complexes based on nitrile[44,48,49] or isocyanide[39,50−55] ligands have attracted a great deal of interest as components in luminescent chromophores. The behavior, as sensors, of the Magnus-type double-salts $[Pt(CNR)_4][Pt(CN)_4]$ (R = alkyl, aryl)[50,56−61] or mixed compounds $[cis\text{-}Pt(CN)_2(CNR)_2]$[50,54] originated by thermal reorganization of the corresponding double salts is noteworthy. The recent studies on $[cis\text{-}Pt(CN)_2(CN\text{-}t\text{-}Bu)_2]$ showing the formation of very luminescent 1D nanomaterials[62] are of great interest.

Finally, we focus attention on the study of the effect of the counteranion (ClO_4^- or PF_6^-) on the electronic absorption and emission spectra of benzoquinolinate bis(isocyanide)platinum(II) complexes.[63]

Results and Discussion

Synthesis and Characterization of $[Pd(C^N)(NCMe)_2]ClO_4$ [C^N = bzq (1), ppy (2)]. Compounds **1** and **2** were prepared by treatment of a suspension of the corresponding dinuclear chloride compounds $[\{Pd(C^N)(\mu\text{-}Cl)\}_2]$ [C^N = bzq

(20) Mdleleni, M. M.; Bridgewater, J. S.; Watts, R. J.; Ford, P. C. *Inorg. Chem.* **1995**, *34*, 2334.
(21) Balashev, K. P.; Puzyk, M. V.; Kotlyar, V. S.; Kulikova, M. V. *Coord. Chem. Rev.* **1997**, *159*, 109.
(22) Lu, W.; Mi, B. X.; Chan, M. C. W.; Hui, Z.; Zhu, N.; Lee, S. T.; Che, C. M. *Chem. Commun.* **2002**, 206.
(23) DePriest, J.; Zheng, G. Y.; Goswami, N.; Eichhorn, D. M.; Woods, C.; Rillema, D. P. *Inorg. Chem.* **2000**, *39*, 1955.
(24) Zheng, G. Y.; Rillema, D. P. *Inorg. Chem.* **1998**, *37*, 1392.
(25) Craig, C. A.; Garces, F. O.; Watts, R. J.; Palmans, R.; Frank, A. J. *Coord. Chem. Rev.* **1990**, *97*, 193.
(26) Xiang, H. F.; Lai, S. W.; Lai, P. T.; Che, C. M. Phosphorescent platinum(II) materials for OLED applications. In *Highly Efficient OLEDs with Phosphorescent Materials*; Yersin, H., Ed.; Wiley-VCH: Weinheim, 2007.
(27) Williams, J. A. G.; Develay, S.; Rochester, D. L.; Murphy, L. *Coord. Chem. Rev.* **2008**, *252*, 2596.
(28) Evans, R. C.; Douglas, P.; Winscom, C. J. *Coord. Chem. Rev.* **2006**, *250*, 2093.
(29) LaDeda, M.; Ghedini, M.; Aiello, I.; Pugliese, T.; Barigelletti, F.; Accorsi, G. *J. Organomet. Chem.* **2005**, *690*, 857.
(30) Neve, F.; Crispini, A.; Campagna, S. *Inorg. Chem.* **1997**, *36*, 6150.
(31) Schwarz, R.; Gliemann, G.; Jolliet, P.; von Zelewsky, A. *Inorg. Chem.* **1989**, *28*, 742.
(32) Neve, F.; Crispini, A.; Di Pietro, C.; Campagna, S. *Organometallics* **2002**, *21*, 3511.
(33) Song, D.; Wu, Q.; Hook, A.; Kozin, I.; Wang, S. *Organometallics* **2001**, *20*, 4683.
(34) Wu, Q.; Hook, A.; Wang, S. *Angew. Chem., Int. Ed.* **2000**, *39*, 3933.
(35) Lai, S. W.; Cheung, T. C.; Chan, M. C. W.; Cheung, K. K.; Peng, S. M.; Che, C. M. *Inorg. Chem.* **2000**, *39*, 255.
(36) Maestri, M.; Sandrini, D.; Balzani, V. *Helv. Chim. Acta* **1988**, *71*, 134.
(37) Maestri, M.; Sandrini, D.; Balzani, V.; von Zelewsky, A.; Deuschel-Cornioley, C.; Jolliet, P. *Helv. Chim. Acta* **1988**, *71*, 1053.
(38) Puzyk, M. V.; Antonov, N. V.; Ivanov, Y. A.; Balashev, K. P. *Opt. Spectrosc.* **1999**, *87*, 277.
(39) Lu, W.; Chan, M. C. W.; Cheung, K. K.; Che, C. M. *Organometallics* **2001**, *20*, 2477.
(40) Yam, V. W. W.; Chan, K. H. Y.; Wong, K. M. C.; Zhu, N. *Chem.−Eur. J.* **2005**, *11*, 4535.
(41) Büchner, R.; Cunningham, C. T.; Field, J. S.; Haines, R. J.; McMillin, D. R.; Summerton, G. C. *J. Chem. Soc., Dalton Trans.* **1999**, 711.
(42) Bailey, J. A.; Hill, M. G.; Marsh, R. E.; Miskowski, V. M.; Schaefer, W. P.; Gray, H. B. *Inorg. Chem.* **1995**, *34*, 4591.
(43) McMillin, D. R.; Moore, J. J. *Coord. Chem. Rev.* **2002**, *229*, 113.
(44) Büchner, R.; Field, J. S.; Haines, R. J.; Cunningham, C. T.; McMillin, D. R. *Inorg. Chem.* **1997**, *36*, 3952.
(45) Yu, C.; Wong, K. M. C.; Chan, K. H. Y.; Yam, V. W. W. *Angew. Chem., Int. Ed.* **2005**, *44*, 791.
(46) Fernández, S.; Forniés, J.; Gil, B.; Gómez, J.; Lalinde, E. *Dalton Trans.* **2003**, 822.
(47) Forniés, J.; Fuertes, S.; López, J. A.; Martín, A.; Sicilia, V. *Inorg. Chem.* **2008**, *47*, 7166.
(48) Chan, C. W.; Lai, T. F.; Che, C. M.; Peng, S. M. *J. Am. Chem. Soc.* **1993**, *115*, 11245.
(49) Blanton, C. B.; Murtaza, Z.; Shaver, R. J.; Rillema, D. P. *Inorg. Chem.* **1992**, *31*, 3230.
(50) Buss, C. E.; Mann, K. R. *J. Am. Chem. Soc.* **2002**, *124*, 1031.
(51) Lai, S. W.; Lam, H. W.; Lu, W.; Cheung, K. K.; Che, C. M. *Organometallics* **2002**, *21*, 226.
(52) Lai, S. W.; Chan, M. C. W.; Wang, Y.; Lam, H. W.; Peng, S. M.; Che, C. M. *J. Organomet. Chem.* **2001**, *617−618*, 133.
(53) Lai, S. W.; Chan, M. C. W.; Cheung, K. K.; Che, C. M. *Organometallics* **1999**, *18*, 3327.
(54) Dylla, A. G.; Janzen, D. E.; Pomije, M. K.; Mann, K. R. *Organometallics* **2007**, *26*, 6243.
(55) Zhou, X.; Zhang, H. X.; Pan, Q. J.; Li, M. X.; Wang, Y.; Che, C. M. *Eur. J. Inorg. Chem.* **2007**, 2181.
(56) Daws, C. A.; Exstrom, C. L.; Sowa, J. R.; Mann, K. R. *Chem. Mater.* **1997**, *9*, 363.
(57) Drew, S. M.; Janzen, D. E.; Buss, C. E.; MacEwan, D. I.; Dublin, K. M.; Mann, K. R. *J. Am. Chem. Soc.* **2001**, *123*, 8414.
(58) Exstrom, C. L.; Pomije, M. K.; Mann, K. R. *Chem. Mater.* **1998**, *10*, 942.
(59) Kunugi, Y.; Mann, K. R.; Miller, L. L.; Exstrom, C. L. *J. Am. Chem. Soc.* **1998**, *120*, 589.
(60) Drew, S. M.; Manna, J. E.; Marquardt, B. J.; Mann, K. R. *Sens. Actuators, B* **2004**, *97*, 304.
(61) Buss, C. E.; Anderson, C. E.; Pomije, M. K.; Lutz, C. M.; Britton, D.; Mann, K. R. *J. Am. Chem. Soc.* **1998**, *120*, 7783.
(62) Sun, Y.; Ye, K.; Zhang, H. X.; Zhang, J.; Zhao, L.; Li, B.; Yang, G.; Yang, B.; Wang, Y.; Lai, S. W.; Che, C. M. *Angew. Chem., Int. Ed.* **2006**, *45*, 5610.
(63) Eryazici, I.; Moorefield, C. N.; Newkome, G. R. *Chem. Rev.* **2008**, *108*, 1834.

Scheme 1

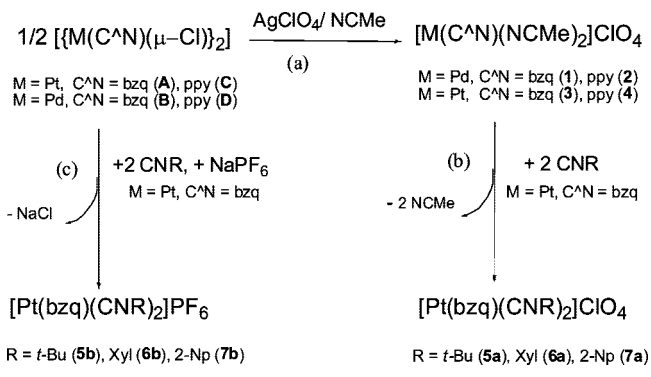

Scheme 2. Numerical Scheme for NMR Purposes

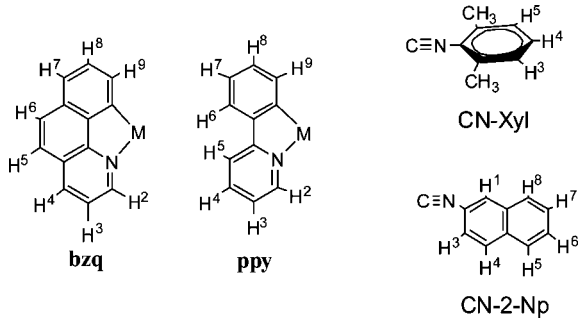

(**B**), ppy (**D**)] with $AgClO_4$ in a 1:2 molar ratio in MeCN. After removing the AgCl, both compounds were obtained from their corresponding solutions as white, analytically pure solids (see Scheme 1, path a, and Experimental Section). Compounds $[Pt(C^N)(NCMe)_2]ClO_4$ [C^N = bzq (**3**), ppy (**4**)] were prepared in the same way as **1** and **2**, as reported earlier.[47] Conductivity measurements on **1** and **2** in acetonitrile confirm their behavior as 1:1 electrolytes.[64] Their IR spectra show the expected absorptions due to the perchlorate (Td) anion[65] and the σ-donor N-coordinated acetonitrile molecules in a *cis* disposition.[66,67] They were characterized by NMR spectroscopy in acetonitrile solutions (see Scheme 2 and Experimental Section). The correct assignment of the eight aromatic protons was made on the basis of 2D NMR $^1H-^1H$ COSY experiments. It is worth noting that both complexes show only one signal at 1.99 ppm (6H) probably due to the lability of acetonitrile ligands. This fact contrasts with the two different signals at $\delta \approx 1.99$ (3 H) and 2.65 (3 H) observed in the analogous platinum compounds (**3** and **4**). This behavior has been previously observed in other related acetonitrile palladium complexes,[68] being attributed to the lower kinetic inertness of palladium(II) complexes with respect to the platinum ones in substitution processes.[69] Compound **3** was used as a starting material in the synthesis of the isocyanide derivatives described below.

Synthesis and Characterization of $[Pt(bzq)(CNR)_2]X$ [R = *t*-Bu, Xyl, 2-Np; X = ClO_4^-, PF_6^-]. The cationic species $[Pt(bzq)(CNR)_2]^+$ were isolated as the ClO_4^- and PF_6^- compounds through two different paths (see Scheme 1, paths b and c, and Experimental Section). Replacement of the acetonitrile molecules in $[Pt(bzq)(NCMe)_2]ClO_4$ **3** with 2 equiv of the corresponding CNR ligands in methanol affords the perchlorate salts $[Pt(bzq)(CNR)_2]ClO_4$ [R = *t*-Bu (**5a**), Xyl (**6a**), 2-Np (**7a**)] in very high yield (>90%). By contrast, compounds $[Pt(bzq)(CNR)_2]PF_6$ [R = *t*-Bu (**5b**), Xyl (**6b**), 2-Np (**7b**)] were prepared in a one-pot reaction by treatment of $[\{Pt(C^N)(\mu\text{-}Cl)\}_2]$ (**A**) with 4 equiv of CNR and 2 equiv of $NaPF_6$ in acetone. All of these compounds were isolated with a similar appearance of yellow solids that were air stable for long periods (months). All compounds have been fully characterized both in the solid state and in solution (see Experimental Section). They show the expected $[Pt(bzq)(CNR)_2]^+$ peak (100%), and their conductivity measurements (nitromethane or acetonitrile) confirm their behavior as 1:1 electrolytes.[64] The proton NMR spectra (assigned on the basis of $^1H-^1H$ COSY experiments) do not vary significantly with the anion and exhibit the expected signals for the bzq and CNR ligands. The $^3J_{Pt-H2}$ values for compounds **5**−**7** [34.5−37.8 Hz] are smaller than that found in compound $[Pt(bzq)(NCMe)_2]ClO_4$ (**3**) (46 Hz), in agreement with the stronger *trans* influence of C (CNR) with respect to N (NCMe).[70] Well-resolved $^{13}C\{^1H\}$ NMR spectra are also observed for complexes **5b** and **6b** (except for the Pt-*C*NR resonance; see Experimental Section for details). The ^{195}Pt NMR nucleus for the *tert*-butyl isocyanide derivative **5b** (δ −4246) is slightly more shielded in relation to the CN-Xyl derivative (δ −4168 **6b**), a feature that could be related to the presence of the electron-withdrawing xylyl ring in **6b**. The IR spectra show two absorptions at about 2200 cm^{-1} due to $\nu(C\equiv N)$, which appear, as expected, shifted to higher frequencies with respect to the corresponding free ligands (CN-*t*-Bu: 2125 cm^{-1}, CN-Xyl: 2131 cm^{-1}, CN-2-Np: 2123 cm^{-1}) similar to that reported for complexes with terminal isocyanide ligands.[39,50−52,54,61,71,72]

Single crystals of compounds **6a** and **6b** were obtained and studied by X-ray crystallography (Figures 1 and 2). Selected bond parameters are given in Table 1. In both cations, the platinum(II) center exhibits a distorted square-planar environment due to the small bite angle of the cyclometalated ligand (bzq) [81.57(9)° in **6a** and 81.37(8)° in **6b**]. This angle and the $Pt-N_{C^N}$ and $Pt-C_{C^N}$ bond lengths are similar to those observed for other bzq platinum compounds.[17−19,46] Two xylylisocyanide ligands complete the coordination sphere of platinum(II). The $Pt-C_{CNXyl}$ bond lengths are comparable to those observed in other Pt(II) isocyanide complexes,[39,50−52,54,62,72−74] the distances *trans* to N_{C^N} being slightly shorter, in agreement with the smaller *trans* influence of the nitrogen atom relative to the metalated carbon atom. The CN-Xyl ligands are almost linearly coordinated, and the deviation from ideal angles is highest in the CN-Xyl *trans* to C_{C^N} in **6a**. In both molecules, one of the CN-Xyl groups is not coplanar with the Pt coordination plane, forming dihedral angles of 70.2° **6a** (CN-Xyl *trans* to C_{C^N}) and 53.0° **6b** (CN-Xyl *trans* to N_{C^N}), respectively. In both complexes, the cations are arranged as head-to-tail dimers through moderate intermolecular $\pi-\pi$ interactions[2,6,13,32,39,75−79] between bzq ligands, which are stronger in **6a** (3.30 vs 3.45 Å **6b**) (Figures

(64) Geary, W. J. *Coord. Chem. Rev.* **1971**, *81*, 7.
(65) Hathaway, B. J.; Underhill, A. E. *J. Chem. Soc.* **1961**, 3091.
(66) Storhoff, B. N.; Lewis, H. C., Jr. *Coord. Chem. Rev.* **1977**, *23*, 1.
(67) Ford, P. C.; Clarke, R. E. *J. Chem. Soc., Dalton Trans.* **1968**, 1109.
(68) Forniés, J.; Navarro, R.; Sicilia, V. *Polyhedron* **1988**, *7*, 2659.
(69) Cotton, F. A.; Wilkinson, G.; Murillo, C. A.; Bochmann, M. *Advanced Inorganic Chemistry*, 6th ed.; Wiley-Interscience: New York, 1999.
(70) Casas, J. M.; Forniés, J.; Fuertes, S.; Martín, A.; Sicilia, V. *Organometallics* **2007**, *26*, 1674.
(71) Chang, X.; Lee, K.-E.; Jeon, S.; Kim, Y.-J.; Lee, H.-K.; Lee, S. W. *Dalton Trans.* **2005**, 3722.
(72) Vicente, J.; Arcas, A.; Fernández-Hernández, J. M.; Aullón, G.; Bautista, D. *Organometallics* **2007**, *26*, 6155.
(73) Bois, H.; Connelly, N. G.; Crossley, J. G.; Guillorit, J. C.; Lewis, G. R.; Orpen, A. G.; Thornton, P. *J. Chem. Soc., Dalton Trans.* **1998**, 2833.
(74) Martellaro, P. J.; Hurst, S. K.; Larson, R.; Abbott, E. H.; Peterson, E. S. *Inorg. Chim. Acta* **2005**, *358*, 3377.
(75) Janiak, C. *J. Chem. Soc., Dalton Trans.* **2000**, 3885.
(76) Hunter, C. A.; Sanders, J. K. M. *J. Am. Chem. Soc.* **1990**, *112*, 5525.
(77) Steed, J. W., Atwood, J. L., Eds. *Supramolecular Chemistry*; Wiley-Interscience: Chichester, 2000.

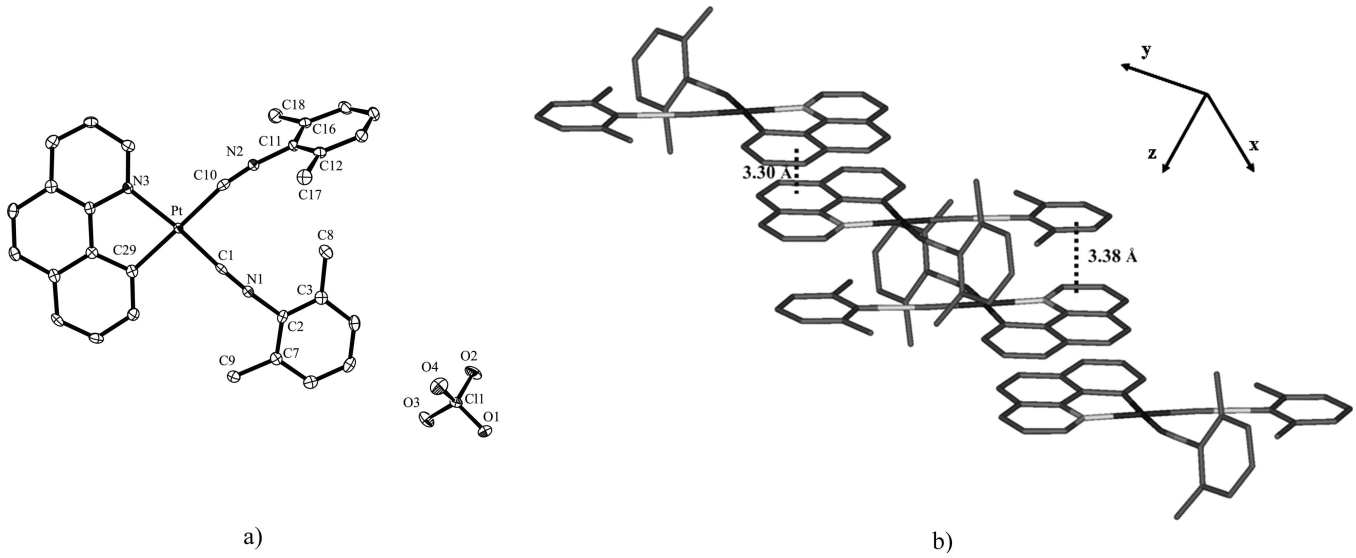

Figure 1. (a) Molecular structure of complex $[Pt(bzq)(CN\text{-}Xyl)_2]ClO_4$ (**6a**). Ellipsoids are drawn at the 50% probability level. Hydrogen atoms are omitted for clarity. (b) View of the stacking of the cations showing the $\pi-\pi$ interactions.

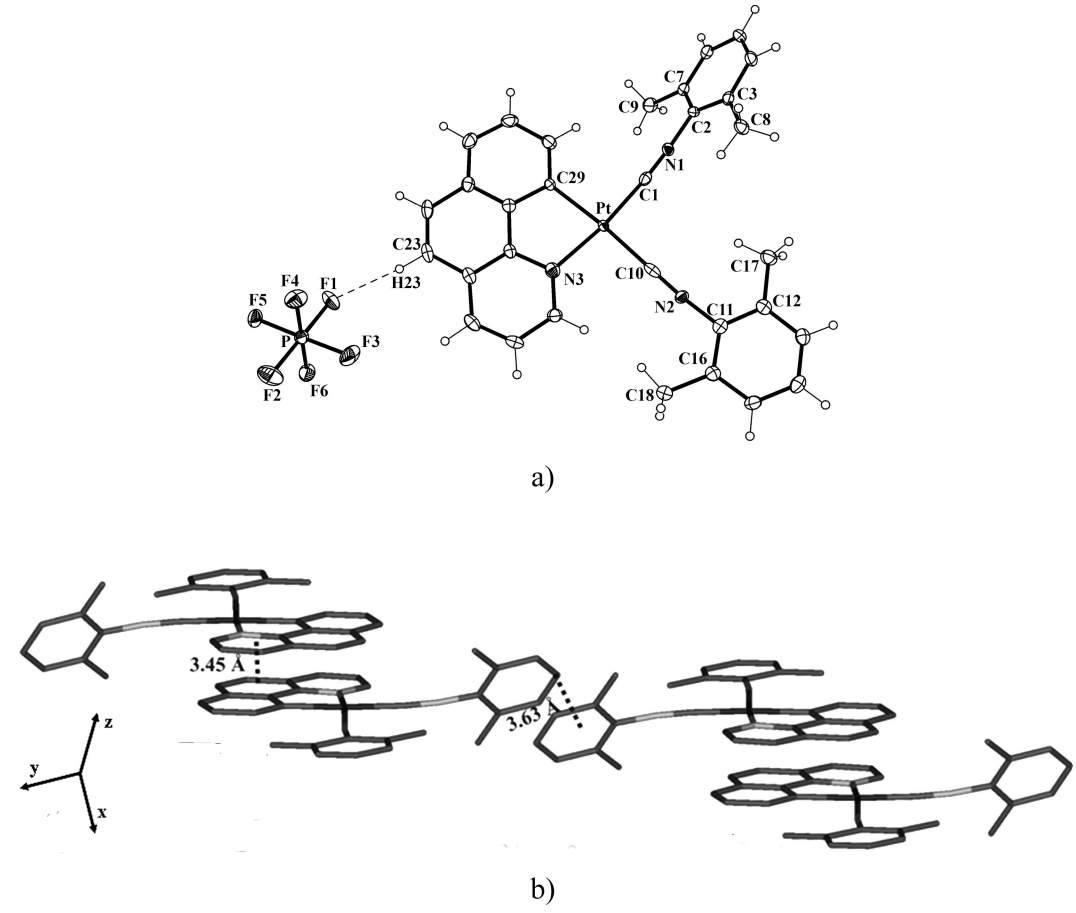

Figure 2. (a) Molecular structure of complex $[Pt(bzq)(CN\text{-}Xyl)_2]PF_6$ (**6b**). Ellipsoids are drawn at the 50% probability level. (b) View of the stacking of the cations showing the $\pi-\pi$ interactions.

1b and 2b). In **6a**, neighboring dimers are arranged in such a way that the xylyl ring of the coplanar group overlaps with one bzq ligand (3.38 Å). For **6b**, the shortest interaction between dimers is found between the xylyl rings of the isocyanide groups, which are not coplanar (~3.63 Å) with the platinum coordination plane. As is shown in Figure 2a, in this compound (**6b**), weak contacts between the anion (PF_6^-) and the cation are observed, with the shortest $P-F\cdots H_{(bzq)}$ distance found being ca. 2.28 Å ($F\cdots H-C$ 164.1°). Despite the differences reported in the crystal packing due to the influence of the counteranion, both crystals have a similar yellow color, in accordance with the very long $Pt\cdots Pt$ distances (4.91(1) Å **6a**, 5.47(1) Å **6b**).

(78) Houlding, V. H.; Miskowski, V. M. *Coord. Chem. Rev.* **1991**, *111*, 145.
(79) Connick, W. B.; Marsh, R. E.; Schaefer, W. P.; Gray, H. B. *Inorg. Chem.* **1997**, *36*, 913.

Table 1. Selected Bond Lengths [Å] and Angles [deg] for 6a·CH_2Cl_2 and 6b·CH_2Cl_2

	6a·CH_2Cl_2	6b·CH_2Cl_2
Pt−C(1)	1.916(3)	1.956(2)
Pt−C(10)	2.013(3)	1.970(3)
Pt−C(29)	2.034(2)	2.051(2)
Pt−N(3)	2.059(2)	2.049(2)
N(1)−C(1)	1.149(3)	1.149(3)
N(1)−C(2)	1.400(3)	1.409(3)
N(2)−C(10)	1.150(3)	1.159(3)
N(2)−C(11)	1.410(3)	1.399(3)
C(1)−Pt−C(10)	88.20(10)	92.98(9)
C(1)−Pt−C(29)	93.16(10)	91.78(8)
C(10)−Pt−N(3)	97.23(9)	93.87(8)
C(29)−Pt−N(3)	81.57(9)	81.37(8)
C(1)−N(1)−C(2)	175.6(2)	174.5(2)
C(10)−N(2)−C(11)	171.3(3)	175.4(2)
N(1)−C(1)−Pt	176.6(2)	175.3(2)
N(2)−C(10)−Pt	169.5(2)	179.7(2)

Absorption Spectra and Theoretical Calculations. Compounds **1**−**4** show low solubility and stability in common organic solvents (dichloromethane, acetone, methanol), except in acetonitrile, in which the electronic absorption spectra were carried out (Figure 3, ∼10^{-4} M; see also Table 2). With reference to previous assignments in analogous C,N-cyclometalated platinum and palladium(II) complexes reported earlier,[2,4−12,14−25,36,80] the high-energy intense bands (λ < 325 nm, ε > 10^4 M^{-1} cm^{-1}) are assigned to metal-perturbed, ligand-centered transitions (^{1}LC $\pi-\pi^*$)[17−20,36] within the bzq or ppy ligands, while the less intense low-energy absorptions (λ > 325 nm) are tentatively ascribed to a mixture of spin-allowed metal-to-ligand charge transfer (^{1}MLCT) and ligand-centered ^{1}LC(bzq) transitions. We note that recent studies on related anionic compounds such as $(NBu_4)[Pt(bzq)(CN)_2]$[47] and $(NBu_4)[Pt(bzq)(C{\equiv}CPh)_2]$[46] suggest that the lower energy bands are described as a mixture of ^{1}MLCT/^{1}LC or ^{1}MLCT/^{1}LL′CT transitions, respectively. In agreement with the partial ^{1}MLCT character associated with these transitions,[17,30,33,81] a remarkable blue shift is observed in the palladium complexes (**1** and **2**) in comparison to those of the analogous platinum ones (**3** and **4**). As shown in Figure 3, the lowest energy band in the benzoquinolinate complexes **1** and **3** is bathochromically shifted in relation to that of **2** and **4** due to the presence of a more extended conjugation in the bzq ligand relative to the phenylpyridinate group.[18,23]

The solid-state diffuse reflectance UV−vis spectra show differences with respect to those observed in acetonitrile solution (see Figure S1), especially **3** (orange color), which exhibits a band with a maximum at 475 nm, assigned to a combination of ^{1}MMLCT [dσ^*(Pt) → π^*(C^N)] and $\pi-\pi^*$ transitions due to Pt···Pt and $\pi-\pi$ stacking interactions among monomers.[2,6,14,78] We note that the solid-state UV−vis absorptions for complex $[Pt(ppy)(NCMe)_2]CF_3SO_3$ have been attributed to ligand-centered $\pi-\pi^*$ transitions.[82]

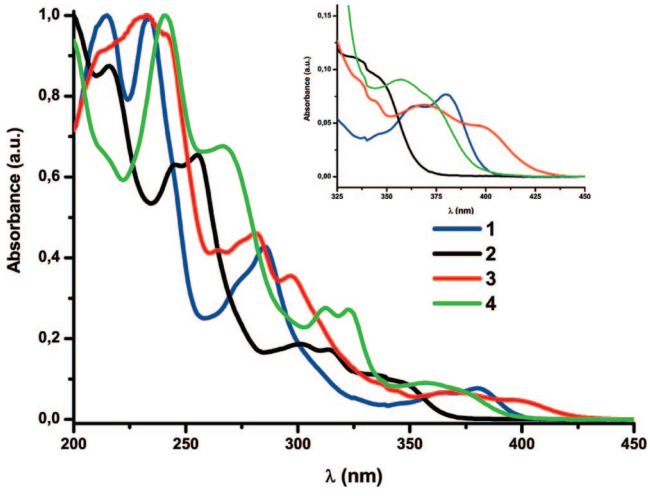

Figure 3. Normalized UV−vis absorption spectra of **1**−**4** in acetonitrile (10^{-4} M).

Due to solubility reasons, the UV−vis spectra of the isocyanide complexes **5** and **6** have been examined only in CH_2Cl_2, DMF, and MeCN and for **7** in DMF and MeCN (see Table 2). The electronic spectra of these compounds in solution (∼10^{-4} M) show no dependence on the counteranion. In addition, as can be observed in Figure S2a, which includes the spectra of the perchlorate derivatives (**5a**−**7a**) in acetonitrile, the influence of the corresponding isocyanide substituent in the low-energy bands is minimal (Table 2), thus suggesting a very low contribution of the co-ligands on the HOMO. These absorptions (>350 nm) are conventionally assigned to a spin-allowed metal-to-ligand charge tranfer ^{1}MLCT [dπ(Pt)→π^*(bzq)] transition, although, as commented above, a ligand-centered ^{1}LC(bzq) contribution cannot be excluded and overlapping with spin-forbidden transitions is also possible.

To shed some light, TD-DFT calculations have been carried out for cation $\mathbf{6}^+$ using B3LYP hybrid functional theory, which agree well with the experimental structure (see Figure S3 and Table S1 for details), the most remarkable difference being that both Xyl rings are nearly perpendicular to the platinum coordination plane. The molecular orbitals involved in the main excited states have been drawn in Figure S4, and the relative compositions of the different energy levels in terms of composing fragments are reported in Table 3. As can be seen in Figure 4a and Table 3, the HOMO is primarily composed of the bzq ligand (93%) with some contribution of the Pt center, while the LUMO consists mainly of the bzq ligand (72%) with some contribution of Pt(5dπ) (12%) and CN-Xyl ligand (16%) orbitals. The calculated excited states in acetonitrile solution (the first eight singlets and four triplets) are listed in Table S2, and the selected allowed transitions are shown (bars) together with experimental absorption maxima in Figure 4b. Calculations indicate that there is a considerable orbital mixing for the transitions, and only a maximum at 384 nm is predicted, which agree roughly with the observed low-energy maximum (∼398 nm **6b**). The major contribution to this band (∼90%) involves the HOMO→LUMO transition, suggesting a remarkable ligand-centered (^{1}LC bzq) character mixed with small ^{1}MLCT character. This assignment is consistent with the modest negative solvatochromism observed for complexes **5**−**7** on going from the least to the most polar solvent investigated (CH_2Cl_2, DMF, and MeCN) (see Table 2 and Figure S5a). In the solvents investigated, the lowest energy absorption band at ca. 400 nm for the six complexes follows Beer's law in the concentration range from 5 × 10^{-5} to 10^{-3} M, suggesting that no remarkable aggregation occurs within this concentration range (see Figure S2b for complex **7b** in MeCN). However, a much weaker band (ε ∼ 20 M^{-1} cm^{-1}) is barely discernible at lower energy in very concentrated solutions (10^{-2} M) in CH_2Cl_2, DMF, and MeCN for the *tert*-butyl and xylylisocyanide derivatives (Figure S5b for **6b**). For the naphthylisocyanide complexes (only soluble at this concentration in DMF), it might be obscured by the tail

(80) Kvam, P. I.; Puzyk, M. V.; Cotlyr, V. S.; Balashev, K. P.; Songstad, J. *Acta Chem. Scand.* **1995**, *49*, 645.
(81) Pérez, S.; López, C.; Caubet, A.; Bosque, R.; Solans, X.; Bardía, M. F.; Roig, A.; Molins, E. *Organometallics* **2004**, *23*, 224.
(82) Burney, J. R. Ph.D., University of Minnesota, 2006, ISBN 976-0-542-89002-4.

Table 2. Absorption Data for Compounds 1−7 at Room Temperature

compound	λ_{abs}/nm (10^3 ϵ M^{-1} cm^{-1}) (solution ~10^{-4} M)	λ_{abs}/nm (solid)
$[Pd(bzq)(NCMe)_2]ClO_4$ (**1**)	215 (39), 234 (38.8), 275 (13.6),285 (16.7), 348 sh (15.9), 365 (2.8), 380 (3) **MeCN**	308, 375
$[Pd(ppy)(NCMe)_2]ClO_4$ (**2**)	217 (27.1), 245 (19.5), 255 (20.3), 301 (5.7), 313 (5.3), 338 (3.3) **MeCN**	260−350
$[Pt(bzq)(NCMe)_2]ClO_4$ (**3**)	212 (33.8), 232 (37.1), 241 (35.4), 265 (15.5), 281 (17.1), 297 (13.2), 369 (2.5), 397 (1.7) **MeCN**	312, 402, 475
$[Pt(ppy)(NCMe)_2]ClO_4$ (**4**)	241 (24.8), 266 (16.7), 312 (6.8), 323 (6.7), 357 (2.2), 375 sh (1.6) **MeCN**	300−380
$[Pt(bzq)(CN\text{-}t\text{-}Bu)_2]ClO_4$ (**5a**)	235 (57.5), 250 (29.3), 256sh (26.3), 288sh (19.6), 300 (23.4), 345 (2.0), 385 (2.9), 402 (2.9) **CH_2Cl_2** 267(15.5), 284sh (22.2), 298 (27.3), 340 (2.4), 380 (3.2), 396 (3.5) **DMF** 209 (29.48), 229 (40.3), 248 (24.6), 285sh (16.4), 295 (19.5), 338 (1.6), 378 (2.3), 395 (2.4) **MeCN**	300, 385, 400, 465
$[Pt(bzq)(CN\text{-}t\text{-}Bu)_2]PF_6$ (**5b**)	220sh (8.4), 235 (29.8), 250 (26.5), 285sh (17.8), 298 (21.5), 343 (1.5), 382 (2.4), 402 (2.6) **CH_2Cl_2** 259 (21.2), 286sh (13.9), 298 (17.4), 380 (0.8), 398 (1.3) **DMF** 210 (25.4), 234 (30.8), 250 (25.8), 280 (16.8), 295 (20.7), 375 (2.6), 394 (2.9) **MeCN**	300, 390, 470
$[Pt(bzq)(CN\text{-}Xyl)_2]ClO_4$ (**6a**)	242 (43.5), 252sh (39.2), 290sh (25.9), 302 (27.6), 346 (2.2), 390 (2.9), 404 (2.8) **CH_2Cl_2** 270 (29.8), 288sh (32.6), 293 (33.6), 342 (4.2), 382 (3.8), 401 (4.0) **DMF** 233 (44.1), 281sh (29), 297 (27.8), 340 (2.3), 380 (2.7), 400 (2.8) **MeCN**	308, 380, 400, 465
$[Pt(bzq)(CN\text{-}Xyl)_2]PF_6$ (**6b**)	221sh (18.3), 235 (57.0), 252sh (38.5), 285 (26.4), 300 (24.7), 345 (2.4), 390 (2.7), 405 (2.6) **CH_2Cl_2** 260 (30.0), 285 (18.4), 292 (18.3), 305 (18.7), 340sh (3.3), 400 (2.1) **DMF** 212 (26.2), 235 (30.6), 252 (28.1), 280 (21.6), 295 (22.9), 379 (2.3), 398 (2.5) **MeCN**	310, 400, 465
$[Pt(bzq)(CN\text{-}2\text{-}Np)_2]ClO_4$ (**7a**)	282 (39,7), 308 (38), 340 (10.3), 380 (4.3), 404 (3.8) **DMF** 234 (120), 244 (88.3), 292 (30,9), 310 (27.0), 340sh (6.4), 384 (2.3), 400 (2.5) **MeCN**	320−490
$[Pt(bzq)(CN\text{-}2\text{-}Np)_2]PF_6$ (**7b**)	260 (49.0), 285 (29.6), 294 (27.9), 320sh (18.2), 345sh (4.9), 400 (0.4) **DMF** 235 (132), 244 (99.5), 292 (37.1), 310 (31.7), 342sh (7.5), 380 (3.8), 400 (3.7) **MeCN**	320−490

Table 3. Population Analysis (%) for 6^+

MO	CNXyl	Pt	bzq
L+2	39	11	50
L+1	71	8	21
LUMO	16	12	72
HOMO	1	6	93
H−1	1	2	97
H−2	100	0	0
H−3	91	7	2
H−4	100	0	0
H−5	97	2	1
H−6	2	18	80
H−7	2	84	14
H−8	13	54	33

of the main band. The wavelength of this band is very similar in each case (range CH_2Cl_2: 464−467 nm; DMF: 462−465; MeCN 461−464 nm) and displays a weaker degree of solvatochromism than the more intense band, but following the same order. This band agrees with the first calculated spin-forbidden triplet in 6^+ (~458 nm, Table S2) and could be attributed to the direct population of a triplet state of mixed LL′CT/LC/MLCT character, facilitated by the high spin−orbit coupling associated with the platinum(II) ion. Notwithstanding, the heavy atom effect in the isocyanide complexes **5**−**7** seems to be not very effective not only because the intensity of the band is very weak (only observed at 10^{-2} M) but also due to the fact that all derivatives **5**−**7** exhibit dual emission (fluorescence and phosphorescence) in solution at 298 K (see below).

Concerning the solid state, similar colors of microcrystalline samples of **5**−**7** were observed for different counteranions, and we noted that the λ_{max} for the same complex but with different anions are almost identical. For **5** and **6**, the solid diffuse reflectance UV−vis spectra (Figure S6 for complexes **a**) exhibit two intense low-energy absorptions at similar energy to those seen in solution (382, 402 nm **5a** in solid vs 385 and 402 in CH_2Cl_2). This suggests that the observed (**6**, see Figures 1b and 2b) or possible (**5**) $\pi-\pi$ interactions between monomers have a very small effect in their absorption maxima. By contrast, complexes **7**, having the 2-naphthylisocyanide ligand, display an intense broad profile from 320 to 490 nm, with a long tail extending to 530 nm, which is probably due to the presence of stronger $\pi-\pi$ stacking in the solid microcrystalline samples.

Emission Spectroscopy. The acetonitrile platinum(II) derivatives $[Pt(bzq)(NCMe)_2]ClO_4$ **3** and $[Pt(ppy)(NCMe)_2]ClO_4$ **4** are photoluminescent at low (77 K) and room temperature both in the solid state and in MeCN solution. However, as has been

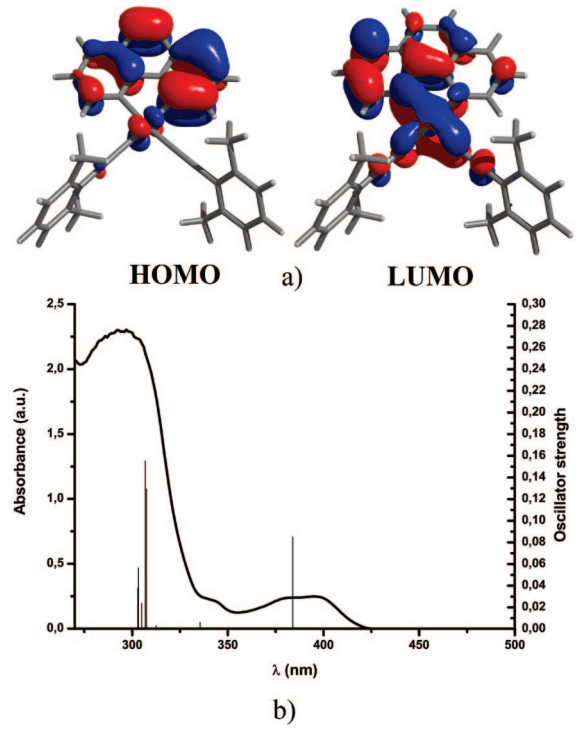

Figure 4. Frontier orbital plots for 6^+ obtained by DFT. Calculated absorption spectrum (bars) of 6^+ in MeCN and experimental UV−vis spectrum of **6b** in MeCN (10^{-4} M) at 298 K.

previously observed in related palladium compounds,[32−38] $[Pd(bzq)(NCMe)_2]ClO_4$ **1** and $[Pd(ppy)(NCMe)_2]ClO_4$ **2** are emissive only at 77 K. This behavior is not unusual in palladium complexes because of the presence of low-lying metal-centered (MC) excited states, which deactivates the potentially luminescent MLCT and LC levels through thermally activated surface-crossing processes.[32] The results are summarized in Table 4. The emission of **4** in fluid (298 K) MeCN solution is not concentration-dependent, exhibiting in the concentration range $10^{-5}-10^{-3}$ M a typical structured emission (478, 512, 543 nm) with vibronic spacing (1389, 1115 cm^{-1}) (Figure 5, 10^{-4} M), consistent with an emission coming from a mixed $^3LC(\pi\pi^*)$/^3MLCT emissive state.[21] In contrast, concentrated solutions of complex **3** (10^{-3} M and 10^{-4} M, Figure 5) result in a high-energy structureless band centered at 437 nm with a very short lifetime (9 ns), by excitation in the range 330−370 nm. However, as shown in Figure S7, the intensity of this emission band decreases with the concentration, being essentially not detectable at 10^{-5} M. The unstructured shape, the short lifetime, and the intensity dependence on the concentration suggest that this emission could be tentatively ascribed to excimer fluorescence.[83] In support of this assignment, its excitation spectrum (367 nm max) differs from that obtained in glass state at 77 K, monitoring at the λ_{max} of the mixed ^3LC/ ^3MLCT emissive state (486 nm).

Interestingly, upon cooling the solutions to the glassy state (77 K), the emission spectra of **1**−**4** are concentration-dependent and very similar to each other (see Figure 6 for complex **4**). In diluted solutions (10^{-5} M, white-cream glasses) all of them exhibit a high-energy structured band, which is ascribed to a typical mixed $^3LC/^3MLCT$ transition of the monomer species. The emission maxima follow the order 460 (**2**) < 471 (**1**) < 476 (**4**) < 486 nm (**3**). This tendency is in accordance with the presence of a higher energy HOMO in platinum derivatives and a lower energy LUMO in the benzoquinolinate complexes, which decreases the energy of the ^3MLCT state. When the concentration increases (10^{-4} and 10^{-3} M, orange glasses), this band disappears and only an unstructured emission maximizing at λ_{max} 680 nm (Pt **3**, **4**), 720 nm (Pd **1**), and 703 nm (Pd **2**), respectively, is observed. As shown in Figure 6, the excitation spectrum corresponding to this new 680 nm emission appears at ca. 480 nm, while the excitation spectrum of the diluted solution (10^{-5} M) monitored at 486 nm (**3**) and 476 nm (**4**) gives rise to a structured high-energy profile, suggesting a different origin for these two emissions. This feature and the change of color of the glasses from cream-white (10^{-5} M) to orange (10^{-3} M) indicate that these low-energy emissions are presumably due to emissive ground-state aggregates generated by M−M (^3MMLCT) and/or $\pi-\pi$ interactions,[4,6,32,39,84] although the existence of excimeric-like emissions cannot be excluded. In agreement with this suggestion, the observed emissions in the solid state are quite similar. Thus, at room temperature (Figure S8), both yellow platinum derivatives, **3** and **4**, show unstructured and symmetrical low-energy, excimeric-like emissions centered at 630 and 595 nm, respectively, which undergo a red shift on cooling (650 **3**, 645 nm **4**). Interestingly, although the white palladium compounds **1** and **2** are not emissive at room temperature in the solid state, cooling at 77 K resulted in a very low-energy and unstructured excimeric emission maximizing at 703 and 690 nm, respectively (Figure S9). It is worth noting that both emissions for **1** and **2** occur at lower energies than in the corresponding platinum solvates **3** and **4**, suggesting stronger interactions between adjacent excited monomers. The observed low-energy emissions in the solid state for **1**−**4** are tentatively attributed to excimeric-like $^3\pi\pi^*$ and/or ^3MMLCT [$\sigma^*(M)\rightarrow\pi^*(C\text{^}N)$] transitions localized on excited interacting adjacent monomers by $\pi-\pi$ and/or M−M interactions. Curiously, in all derivatives the observed emission maximum in the solid state appears blue-shifted with respect to that seen in the rigid glassy acetonitrile solution (Table 4), a fact that is more remarkable in the platinum complexes [**3** (30 nm), **4** (35 nm)]. This behavior seems to indicate that packing of cations and anions in the solid lattice occurs in such a way that it causes a greater separation between interacting adjacent metallic cations than in glassy solutions ($\geq 10^{-4}$ M).

On the basis of the combination of the strong-field cyclometalating ligand and strong-field isocyanide ancillary ligands, high-efficiency luminescence would be expected for the isocyanide complexes **5**−**7**. At room temperature, the behavior of complexes **5a** and **5b** in CH_2Cl_2 solutions ($5 \times 10^{-5}-10^{-3}$ M range) is similar to that of related **6a** and **6b**; therefore only the emission spectra of **5a** and **5b** are presented (Figures 7, 8, and S10). By excitation at $\lambda_{max} > 360$ nm (Figures 7 and S10), all of them show a structured emission band (λ_{max} ~470 **5**, ~475 nm **6**, see Table 4) whose excitation spectra mimic the absorption spectra in the low-energy region, being ascribed to a mixed $^3LC/^3MLCT$ excited state, probably with a remarkable ^3LC character (see below for emission spectra in other solvents). However, excitation at higher energies ($\lambda \leq 330$ nm) results in an additional high-energy structured emission band at 345 nm, along with the $^3LC/^3MLCT$ band at 470 nm. An intermediate additional structureless emission band centered at ca. 430 nm is also observed using concentrated solutions (10^{-3} M) when the counterion is PF_6^- (**5b**, **6b**) or at concentrations up to 5×10^{-5} M when the counterion is ClO_4^- (**5a**, **6a**). Although too weak for lifetime measurements, the high-energy structured emission (345−385 nm) clearly originates from a ligand-centered (bzq) predominantly spin-allowed $^1(\pi\pi^*)$ excited state (fluorescence). Additional support arises from the small Stokes shift between the excitation and emission spectra (see Figure 7 for **5b**) and the fact that this high-energy emission is comparable to that of the free ligand (Hbzq: 349, 366, 385 nm). As can be seen in Figure S10, the excitation spectrum monitoring at the intermediate unstructured band (430 nm) differs from that obtained monitoring the structured high- and low-energy emissions, suggesting a different emissive manifold of difficult assignment. As reported above, this behavior indicates that the intersystem crossing (ISC) and/or internal conversion (IC) between emissive states is probably of low effectiveness at room temperature. Clearly the change of the weakly coordinated NCMe molecules by the stronger σ-donating isonitrile CNR ligands in the "Pt(bzq)" core probably reduces the degree of platinum−benzoquinolinate ($Pt-C_{bzq}$) orbital (σ and π) interactions, which seems to be crucial to the manifestation of the heavy atom effect.[85]

For complex **6a**, the dependence of the lifetime in deaereated CH_2Cl_2 solution measured at 470 nm has been examined. The lifetime decreases slightly in the 2.5×10^{-5} to 10^{-4} M range from 3.08 to 2.67 μs. As can be observed in Figure S11, the observed emission decay rate constants ($K_{obs} = 1/\tau_{obs}$) increase linearly with the concentration, fitting well to the Stern−Volmer equation of the form $K_{obs} = K_o + K_Q[Pt]$, where

(83) Yamaji, M.; Tsukada, H.; Nishimura, J.; Shizuka, H.; Tobita, S. *Chem. Phys. Lett.* **2002**, *357*, 137.

(84) Siemeling, U.; Bausch, K.; Fink, H.; Bruhn, C.; Baldus, M.; Angerstein, B.; Plessow, R.; Brockhinke, A. *Dalton Trans.* **2005**, 2365.

(85) Hu, J.; Yip, J. H. K.; Ma, D. L.; Wong, K. Y.; Chung, W. H. *Organometallics* **2009**, *28*, 51.

Table 4. Emission Data for Complexes 1−7

compound	medium (T[a]/K)	λ_{em}/nm (λ_{exc}/nm)	$\tau/\mu s$[a]
$[Pd(bzq)(NCMe)_2]ClO_4$	solid (77)	703 (425−470)	2.4
(**1**)	MeCN[b] (77)	720 (360−400)	
	MeCN[c] (77)	471, 481sh, 506, 545 (345−385)	
$[Pd(ppy)(NCMe)_2]ClO_4$	solid (77)	690 (350−400)	1.6
(**2**)	MeCN[b] (77)	703 (385)	
	MeCN[c] (77)	460, 483, 494, 521 (330−350)	
$[Pt(bzq)(NCMe)_2]ClO_4$	solid (298)	630 (425−510)	0.2
(**3**)	solid (77)	650 (460−520)	1.5
	MeCN (298)	437 (330−370)	9 ns
	MeCN[b] (77)	680 (425−475)	
	MeCN[c] (77)	486, 523, 564 (350−375)	
$[Pt(ppy)(NCMe)_2]ClO_4$	solid (298)	595 (425−525)	2.3 (68.3%), 0.4 (31.7%)
(**4**)	solid (77)	645 (425−480)	3.3
	MeCN (298)	478, 512, 543 (320−380)	
	MeCN[b] (77)	680 (385−485)	
	MeCN[c] (77)	476, 512, 543 (325−380)	
$[Pt(bzq)(CN\textit{t}\text{-}Bu)_2]ClO_4$	solid (298)	476, 504, 590 (350−450)	57.3 (12.3%), 14.3 (87.7%)
(**5a**)	solid (77)	500, 538max, 575, 620sh (370−460)	1310 (61.3%), 280 (38.7%) (500, 538)
		538, 640 (475)	
		650 (510)	
	CH_2Cl_2[e] (298)	345, 367, 385,430, 470, 502, 534 (300)	2 ns (430)
		430, 470, 502, 534 (360)	10 ns (540)
		470, 502, 534 (400)	
	CH_2Cl_2[e] (77)	502, 535, 582 (330−420)	243 (76.2%), 17.2 (23.8%) (502)
			256 (33.6%), 37.1 (66.4%) (535)
			165 (10.3%), 13.0 (89.7%) (582)
$[Pt(bzq)(CN\textit{t}\text{-}Bu)_2]PF_6$	solid (298)	504max, 535 (360−460)	9.6 (504)
(**5b**)	solid (77)	508max, 545, 590 (360−440)	73.6 (508)
	CH_2Cl_2[e] (298)	345, 367, 385, 410, 470, 502, 543 (280−330)	5 ns (470)
		470, 502, 543 (360−400)	
	CH_2Cl_2[e] (77)	502, 535, 590 (360−400)	469 (502)
$[Pt(bzq)(CN\text{-}Xyl)_2]ClO_4$	solid (298)	475, 485, 500, 540 (360−430)	76.9 (17%), 27.6 (83%) (500)
(**6a**)	solid (77)	498, 536, 580 (350−475)	806 (498)
	CH_2Cl_2[e] (298)	345max, 367, 385, 433max, 476max, 509, 545 (290−310)	
		476max, 509, 545 (400)	
	CH_2Cl_2[e] (77)	506, 535, 615 (300−400)	244 (19.4%), 26.4 (80.6%) (506);
			106.5 (15.5%), 11.9 (84.5%) (615)
$[Pt(bzq)(CN\text{-}Xyl)_2]PF_6$	solid (298)	495, 518, 556 (360−475)	98.4 (495); 89.8 (518); 68.6 (560)
(**6b**)	solid (77)	495, 505, 528, 570 (360−460)	209.3 (495)
	CH_2Cl_2[e] (298)	348, 366, 385, 406sh, 475, 507, 548 (280−320)	
		475, 507, 548 (360−400)	
	CH_2Cl_2[e] (77)	502, 532, 590 (360−420)	141.4 (502)
$[Pt(bzq)(CN\text{-}2\text{-}Np)_2]ClO_4$	solid (298)	635 (500)	0.4 (75.5%), 0.08 (24.5%)
(**7a**)	solid (77)	590 (350−450)	97.9 (9.3%), 26.9 (90.7%) (590)
		590sh, 675 (500)	29.4 (8.1%), 1.8 (91.9%) (675)
	MeCN[d] (298)	666 (367−420)	11.9 (0.3%), 1.9 (99.7%)
	MeCN[d] (77)	690 (500), 735 (540)	2.1 (98.6%), 11.8 (1.4%) 4.0 (94.1%), 12.3 (5.9%)
	MeCN[e] (298)	327, 345, 360 (277) 480 sh, 545, 650 (320−390)	0.4 (5.2%), 3.4 ns (94.8%) (545)
		650 (450)	7.7 ns (650)
	MeCN[e] (77)	741 (540)	3.2
$[Pt(bzq)(CN\text{-}2\text{-}Np)_2]PF_6$	solid (298)	630 (420−500)	4.2 (60%); 0.06 (40%)
(**7b**)	solid (77)	573 (370−420) 573, 685 (500)	149.8
	MeCN[d] (298)	620, 660sh (360−420)	0.9
	MeCN[d] (77)	710 (520) 775 (590)	13.6
	MeCN[e] (298)	330, 345, 364, 380 (280) 394, 400, 416 (360) 480sh, 540, 650sh (400)	
	MeCN[e] (77)	735 (540)	9.4

[a] Air-equilibrated samples. [b] Concentrated (10^{-3}, 10^{-4} M). [c] Diluted (10^{-5} M). [d] 10^{-3} M. [e] 5×10^{-5} M.

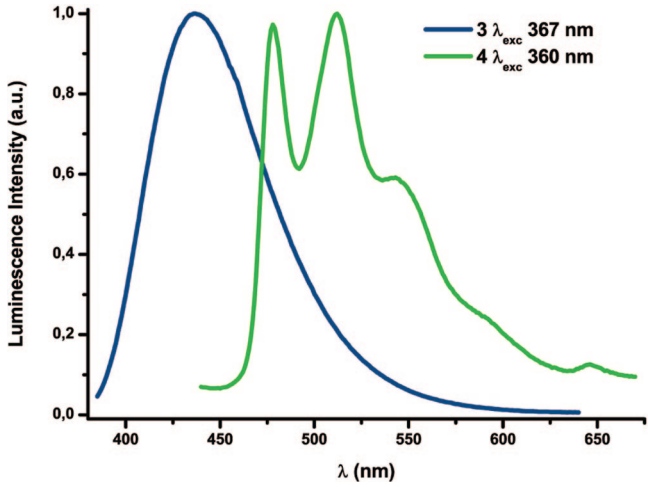

Figure 5. Normalized emission spectra of **3** and **4** in MeCN at 298 K (10^{-4} M).

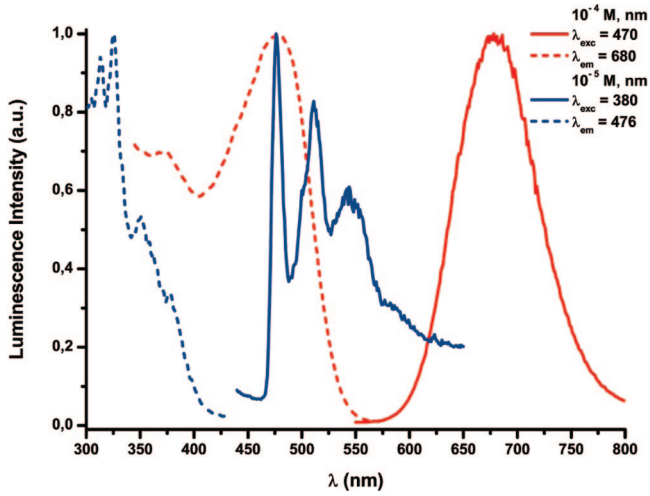

Figure 6. Normalized excitation and emission spectra of **4** in MeCN at 77 K (10^{-4} and 10^{-5} M).

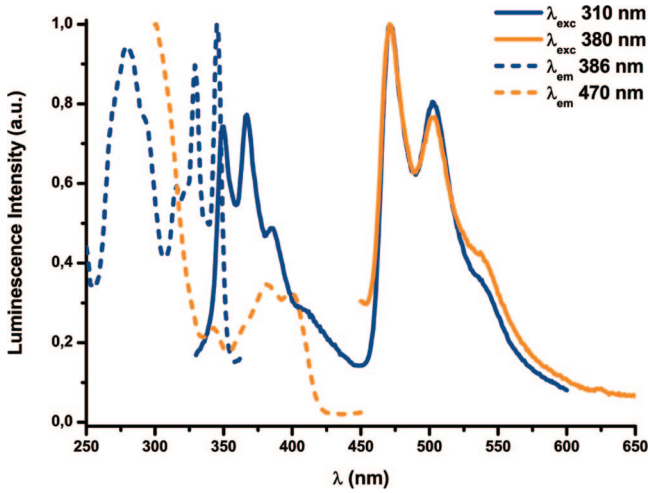

Figure 7. Normalized excitation and emission spectra of **5b** at 298 K in dichloromethane (5×10^{-5} M).

$K_o = (1/\tau_o)$ is the emission rate constant at infinite dilution and $K_Q$is the apparent rate constant of self-quenching,[86,87] which provides an indication of the susceptibility of the complex to self-quench through excimer formation (Figure S11). The lifetime of emission at infinite dilution τ_o is 3.2 μs, and the value of K_Q (0.65 $\times$ 10^9 M^{-1} s^{-1}) (determined from the linear variation of K_{obs} as a function of the concentration) indicate little self-quenching.[16,86,88−90]

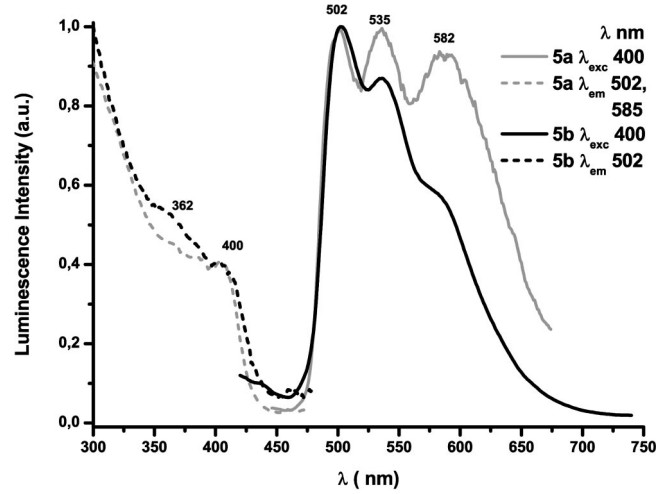

Figure 8. Normalized excitation and emission spectra of **5a** and **5b** at 77 K in dichloromethane (5×10^{-5} M).

An additional solvent-dependent emission study at room temperature in diluted solution (5×10^{-5} M) has been carried out in more polar solvents (DMF and MeCN), and the results are collected in Table S3. It is remarkable that although dual fluorescence ($^1\pi\pi^*$) and phosphorescence (^{3}LC/^{3}MLCT) is still observed in all complexes, the emissions are clearly dominated by the high-energy structured fluorescence bands probably due to the quenching effect of these donor solvents (as an illustration see Figure S12 for complex **5b**). In addition, the intermediate band located at ~430 nm, which is seen in CH_2Cl_2, also disappears in these solvents. Concerning the solvent effect on the maxima (>470 nm), its influence is negligible (Table S2), which is in agreement with emission emanating mainly from a ^{3}LC excited state. Notwithstanding, for **6a** in acetonitrile, a low unstructured feature located at 575 nm ($^3\pi\pi^*$ excimeric in nature) is also observed.

When the CH_2Cl_2 solutions are frozen, $^1(\pi\pi^*)$ fluorescence and intermediate (430 nm) emissions disappear, indicating effective falling to low-lying emissive manifolds. However, while the PF_6^- derivatives (**5b** and **6b**) exhibit only a structured band centered at ca. 502 nm, the ClO_4^- complexes also show the presence of an additional low-energy unstructured manifold (582 **5a**, 615 nm **6a**). As an illustration of this different behavior, the emission spectra of **5a** and **5b** in diluted 5×10^{-5} M solutions at 77 K are shown in Figure 8. Similar spectra were obtained at higher concentrations with the low-energy manifold for **5a** and **6a** being more prominent. For the structured emission of **5b** and **6b**, the absence of rigidochromism, together with the negligible influence of the isocyanide ligand and the extremely long lifetimes, which fit well to monoexponential

(86) Connick, W. B.; Geiger, D.; Eisenberg, R. *Inorg. Chem.* **1999**, *38*, 3264.
(87) Horvath, A.; Stevenson, K. L. *Coord. Chem. Rev.* **1996**, *153*, 57.
(88) Guo, F.; Sun, W.; Liu, Y.; Schanze, K. *Inorg. Chem.* **2005**, *44*, 4055.
(89) Williams, J. A. G.; Beeby, A.; Davies, E. S.; Weinstein, J. A.; Wilson, C. *Inorg. Chem.* **2003**, *42*, 8609.
(90) Develay, S.; Blackburn, O.; Thompson, A. L.; Williams, J. A. G. *Inorg. Chem.* **2008**, *47*, 11129.

decays (air-equilibrated glasses, 469 μs **5b**, 141.4 μs **6b**), is indicative of emission with primarily ^{3}LC parentage. For the ClO_4^- derivatives, lifetime measurements in all maxima always fit to two components (see Table 4). The long component dominant in the high-energy peaks is attributed to the structured ^{3}LC emission, while the short component, which is predominant in the low-energy band, is tentatively attributed to excimeric $^3\pi\pi^*$ emission. In keeping with this notion, the excitation spectra of **5a** monitored at 502 and 585 nm are similar (see Figure 8). It is worth noting that the phosphorescence lifetimes at 77 K (and also in the solid state at 77 K) are longer than at room temperature, suggesting that they are mainly determined by nonradiative decay rates, which usually decrease with lowering temperature.

We have also performed a temperature-dependent study on the luminescence properties of a diluted 5×10^{-5} M deaereated CH_2Cl_2 solution of **5a**. In Figure S13 are collected emission spectra and lifetimes as registered against the temperature in the 298−77 K range. As can be observed, by decreasing slowly the temperature the final emission profile obtained at 77 K is slightly different than that observed by freezing the solution suddenly (Figure S13b vs Figure 8). The most remarkable effect is that the high structured emission decreases in intensity relative to the low-energy excimeric feature and the peak maxima of the ^{3}LC are broader and slightly blue-shifted (490, 528 nm vs 502, 535 nm). It may be noted that the lifetimes measured in the 470−490 band are significantly larger than those obtained in air-equilibrated solution, as would be anticipated due to its triplet parentage. From Figure S13, it can be seen that by cooling from 298 to 173 K, no energetic variation is observed in the dual emission (fluorescence and phosphorescence), but the intensity of the phosphorescence increases remarkably while the fluorescence decreases to a lesser extent. The phosphorescence emission lifetime increases concomitantly, fitting to a monoexponential decay from 298 to ca. 198 K (1.5 μs at 298 K to 51.8 μs at 198 K). At 173 K, which is close to the freezing temperature (177.9 K), the lifetime increases rapidly and fits two components [837.5 μs (55.8%), 256.5 μs (44%)], suggesting the presence of two close emissive states. Below this temperature, the structured emission shows a small bathochromic shift (λ_{max} ~490 nm) and the low-energy unstructured feature ascribed to $^3\pi\pi^*$ excimer emission is observed (~586 nm). Both the presence of a biexponential decay with two very long lifetime components at λ_{max} ~490 nm (similar to those seen in the solid state at 77 K: 1045.9 (55.1%), 129.9 (44.9%) μs glass 77 K; 1310 (61.3%), 280 (38.7%) μs solid 77 K) and the very intense excimer emission below 173 K could be indicative of the existence of a crystallization process. However, we noted that the maxima of both emissions are slightly different. For instance, by exciting at ~450 nm the maximum of excimer emission occurs at 620 nm, which is different from that observed in the solid state at 77 K (~650 nm, Figure S16). The appearance of excimer (or ground-state aggregate) emission at 77 K for glasses but not at room temperature is not unprecendented and indicates that the association constant could be too small to be observed at room temperature.

For **7a** and **7b**, which are not soluble in CH_2Cl_2, the emission spectra were recorded in MeCN (Table 4) and DMF (Table S3), and again, the tendency to form excimers is higher in the ClO_4^- derivative **7a**. Thus, in a diluted MeCN solution (5×10^{-5} M), **7b** exhibits, by excitation in the low-energy absorption (380−400 nm), an asymmetric emission (480sh, 540 nm) ascribed to a mixed ^{3}LC/^{3}MLCT excited state, while excitation at higher energies (280−320 nm) and 360 nm results in additional

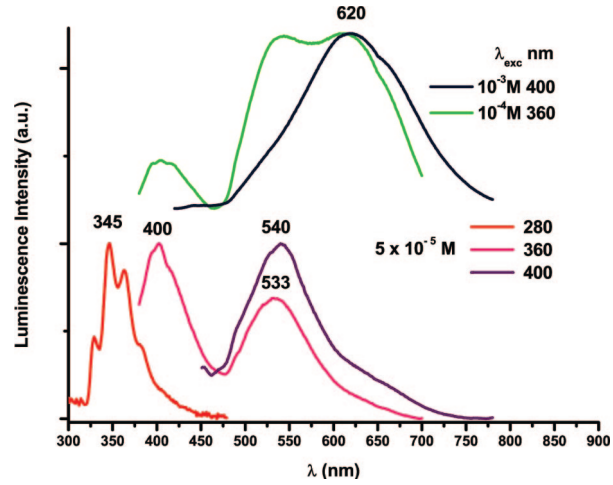

Figure 9. Normalized emission spectra of **7b** in acetonitrile at 298 K at different concentrations.

structured (330, 345, 360, 380 nm) (394, 400, 416 nm) ligand-centered $^1\pi\pi^*$ emissions, with contribution of both bzq and CN-2-Np groups (Figure 9).[91] When the concentration increases (10^{-4}, 10^{-3} M), a new additional low-energy feature, which maximizes at ca. 620 nm by exciting at 400 nm, is observed. Similar behavior is observed for **7a** in MeCN, but in this case the low-energy feature is observed, as for complex **6a** in MeCN, even in a diluted 5×10^{-5} M solution (see Figure S14). As can be seen in Figure S14 for **7a**, the excitation spectra monitored at the low-energy feature are different from that monitored at the high-energy band, suggesting that the broad low-energy band originates from an emissive state resulting from ground-state aggregation of the complexes. In diluted (5×10^{-5} M) DMF solution, the triplet mixed ^{3}LC/^{3}MLCT emission for both complexes **7a** and **7b** is very weak, with emission maxima slightly blue-shifted (~470 nm in DMF vs 480 nm in MeCN). In addition, by excitating at high energy (280−310 nm), the only emission observed (see Table S3) is $^1\pi\pi^*$ fluorescence (330, 345, 364, 380 nm). The tendency to form excimers is lower than in acetonitrile and becomes apparent only at elevated concentrations (~10^{-3} M).

In glassy (77 K) acetonitrile, the emission profile for **7a** and **7b** is similar and also depends on the concentration and the excitation wavelength. Curiously, at low concentration (5×10^{-5} M) only one symmetric structureless band at very low energy (741 nm **7a**, 735 nm **7b**, related to a maximum excitation peak at 540 nm) is observed (see Figure 10 for **7a**). This emission is attributable to ^{3}MMLCT [dσ^*(Pt)→π^*] transitions, probably due to the close distance and interaction between the platinum centers. However, when the concentration increases to 10^{-3} M, the glasses exhibit site-selective emission, presumably due to the simultaneous presence of $^3\pi\pi^*$ and ^{3}MMLCT ^{3}(d$\sigma^*\pi^*$) transitions. Thus, two structureless symmetric bands at 690 nm (λ_{exc} 500 nm) and 735 nm (λ_{exc} 540 nm) for complex **7a** and at 710 nm (λ_{exc} 520 nm) and 775 nm (λ_{exc} 590) for **7b** are seen with 10^{-3} M solutions at 77 K. In both complexes the excitation spectra monitored at the low-energy band (735 nm **7a**, 775 nm **7b**) are distinct from those monitored at the less energetic emission (690 nm **7a**, 710 nm **7b**), indicating their different origin [^{3}(d$\sigma^*\pi^*$) and $^3\pi\pi^*$]. Apparently, in diluted solution glasses, the tendency to selectively form aggregates through

(91) Fluorescence of 2-naphthylisocyanide occurs at 331, 346, 363, and 381 nm.

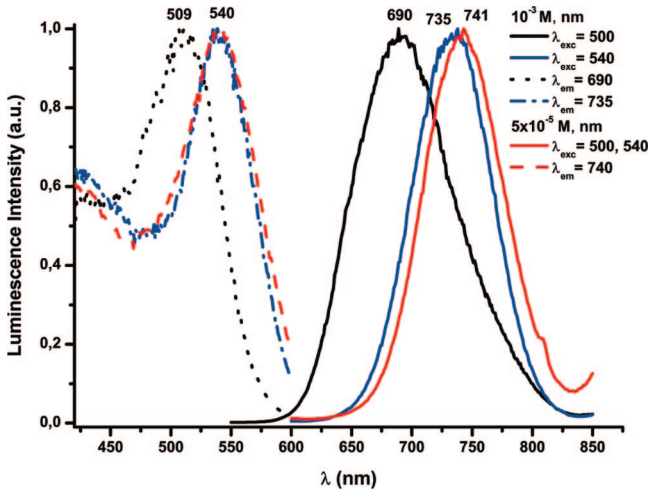

Figure 10. Normalized excitation and emission spectra of **7a** in acetonitrile at 77 K.

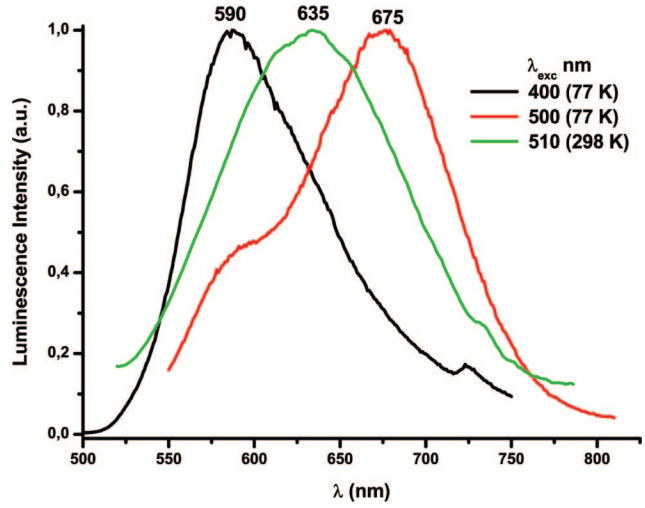

Figure 11. Normalized emission spectra of [Pt(bzq)(CN-2-Np)$_2$]ClO$_4$ **7a** in the solid state.

Pt···Pt interactions is prevalent, while at higher concentrations both $\pi-\pi$ and Pt···Pt emissive dimers and/or oligomers are generated, which is further evident from the emission lifetime measurements listed in Table 4.

The luminescence observed in the solid state for complexes **5**−**7** is quite similar to that observed in glasses at 77 K, and only in the *tert*-butylisocyanide derivatives is the influence of the counteranion clearly visible. Thus, despite the presence of weak $\pi\pi$ stacking interactions found in the solid state (Figures 1 and 2) for the xylylisocyanide derivatives (**6a**, **6b**), these complexes exhibit vibronically structured emissions (298, 77 K) attributed mainly to the ^{3}LC excited state. Notwithstanding this, the emissions at 298 K are broader and their lifetime measurements fit two components, suggesting that a small excimeric character of the emission cannot be excluded (Figure S15). By contrast, the 2-naphthylisocyanide complexes show, at room temperature, an intense broad emission (635 nm **7a**, 630 nm **7b**) attributed to excimeric $^3\pi\pi^*$ excited states. Upon cooling to 77 K, two distinct emissions are resolved depending on the excitation wavelength (see Table 4). As can be observed in Figure 11 for complex **7a**, both emissions (590, 675 nm **7a**; 573, 685 nm **7b**) mimic those observed in concentrated acetonitrile glasses (10^{-3} M, 77 K, see Figure 10), being similarly assigned to $^3\pi\pi^*$ and ^{3}(d$\sigma^*\pi^*$) excited states, respectively. This behavior, together with the reflectance diffuse spectra (Figure S6), suggests that probably both $\pi\pi$ and Pt···Pt contacts are prevalent in the crystal packing of both complexes **7a** and **7b**. The influence of the counterion is observed in the CN-*t*-Bu derivatives. To illustrate this, the emission spectra of **5a** and **5b** are given in Figure S16. **5b** (PF_6^-) exhibits only typical structured profiles (298, 77 K) due to ^{3}LC excited states, while for **5a**, containing the smaller ClO_4^- counterion, additional emission due to excimeric $^3\pi\pi^*$ is also evident, this being predominant at 298 K.

Conclusions

In summary the synthesis and photophysics of a new series of cationic cyclopalladated complexes [Pd(C^N)(NCMe)$_2$]ClO$_4$ (C^N = bzq **1**, ppy **2**), analogous to the previously described platinum complexes (**3**, **4**)[47] and isocyanide platinum derivatives [Pt(bzq)(CNR)$_2$]X (R = *t*-Bu **5**, Xyl **6**, 2-Np **7**; X = ClO_4^- **a**, PF_6^- **b**), are reported. The X-ray crystal structures of **6a** and **6b** reveal the presence of similar $\pi-\pi$ stacking dimers that pack through additional, slightly different, $\pi-\pi$ interactions (bzq/xylyl **6a** or xylyl/xylyl **6b**). Complexes **3** and **4** are strongly emissive in all media (298 and 77 K), whereas the palladium complexes are emissive only in rigid media at 77 K. Curiously in acetonitrile solution complex **3** shows a high-energy unstructured emission band (ascribed to excimeric fluorescence), whereas **4** exhibits a typical structured emission coming from a ^{3}LC($\pi\pi^*$) emissive state with a small amount of the ^{3}MLCT state. At 77 K (glassy solutions), the emission spectra of all acetonitrile complexes **1**−**4** are concentration-dependent, exhibiting typical ^{3}LC/^{3}MLCT structured emissions at low concentration (10^{-5} M) and low-energy excimeric-like $^3\pi\pi^*$ and/or ^{3}MMLCT [dσ^*(Pt) → π^*(C^N)] unstructured bands at higher concentrations, similar to those observed in the solid state at room temperature (**3**, **4**) and at 77 K (**1**−**4**).

On the basis of TD-DFT calculations on $\mathbf{6}^+$, the lowest energy absorption seen in the isocyanide complexes **5**−**7** is suggested to be ^{1}IL in nature mixed with some ^{1}MLCT character. Their emissive properties in fluid solution indicate that intersystem crossing between singlet and triplet states is very inefficient, probably due to the stronger σ-donating properties of the CNR ligands, which reduces the heavy effect atom. Thus, for **5** and **6** in CH_2Cl_2 solutions, three different bands are observed: $^1\pi\pi^*$ fluorescence (345−385 nm), ^{3}LC/^{3}MLCT phosphorescence (λ_{max} ∼470 nm), and a broad structureless emission at ca. 430 nm, whose presence is concentration dependent. The λ_{max} of phosphorescence emission is not particularly sensitive to solvent polarity, but it is considerably quenched in MeCN and DMF. In addition, in these solvents the band at 430 nm is not observed. Emission lifetimes for deaereated CH_2Cl_2 solutions of **5a** reveal little self-quenching, but the presence of oxygen decreases the intensity of the phosphorescence. At 77 K (glassy CH_2Cl_2 solutions), the fluorescence and the intermediate band (430 nm) disappear and for the ClO_4^- derivatives (**5a** and **6a**) phosphorescent excimeric-like $^3\pi\pi^*$ emissions are observed. The emissions of the 2-naphthylisocyanide derivatives (**7**) also exhibit a similar solvent concentration and excitation wavelength dependence both at room and at low (77 K) temperature, the ClO_4^- derivative **7a** being more prone to show excimeric emission. For these complexes (**7**) the low concentrated rigid glasses (5×10^{-5} M) exhibit only one structureless band at very low energy (741 nm **7a**, 735 nm **7b**) due to a ^{3}MMLCT [dσ^*(Pt)→π^*] transition. However, by increasing the concentration (10^{-4}, 10^{-3}

M) of the glassy solutions, an interesting dual site-selective emission (690, 735 nm **7a**; 710, 775 nm **7b**) is clearly observed due to the simultaneous presence of both excimeric $^3\pi\pi^*$ and ^{3}MMLCT transitions. The behavior of these isocyanide complexes (**5**−**7**) in the solid state is similar to the rigid glasses, and it is only in the CN-*t*-Bu derivatives that the influence of the counteranion is visible. In general, the following tendency to exhibit excimeric-like emission ($^3\pi\pi^*$ and/or ^{3}d$\sigma^*\pi^*$) is observed: CN-2-Np > CN-*t*-Bu > CN-Xyl and ClO_4^- > PF_6^-.

Experimental Section

General Considerations. The starting materials [{Pt(bzq)(μ-Cl)}$_2$] (**A**),[92] [{Pd(bzq)(μ-Cl)}$_2$] (**B**),[93] [{Pt(ppy)(μ-Cl)}$_2$] (**C**),[20] and [{Pd(ppy)(μ-Cl)}$_2$] (**D**)[94] were prepared according to reported procedures with slight modifications. The synthesis of [Pt(C^N)(NCMe)$_2$]ClO$_4$ (C^N = bzq **3**, ppy **4**)[47] has been previously reported. The reactions were carried out without precautions to exclude atmospheric oxygen or moisture. *tert*-Butylisocyanide (CN-*t*-Bu), 2,6-dimethylphenylisocyanide (CN-Xyl), and 2-naphthylisocyanide (CN-2-Np) were purchased from commercial suppliers.

Instrumental Methods. Infrared spectra were recorded in the 4000−200 cm^{-1} range on Perkin-Elmer 883 and Nicolet Nexus FT-IR spectrophotometers using Nujol mulls between polyethylene sheets. Conductivities were measured in ca. 5×10^{-4} mol dm^{-3} solutions with a Philips 9509 or a Crison GLP31 conductimeter. C, H, and N analyses were carried out with a Perkin-Elmer 2400 microanalyzer. Mass spectra were recorded on a HP-5989B mass spectrometer (ES technique). UV−visible spectra were obtained on a Hewlet Packard 8453 spectrometer. NMR spectra were recorded on Bruker ARX 300 and Bruker AVANCE 400 spectrometers. Chemical shifts are cited relative to $SiMe_4$ (^{1}H, external), $CFCl_3$ (^{19}F, external), and 85% H_3PO_4 (^{31}P, external) and Na_2PtCl_6 in D_2O (^{195}Pt). *J* are given in Hz, and assignments are based on ^{1}H−^{1}H COSY and gHSQC experiments (for complexes **5b** and **6b**). Diffuse reflectance UV−vis (DRUV) spectra were recorded on a Unicam UV-4 spectrophotometer equipped with a Spectralon RSA-UC-40 Labsphere integrating sphere. The solid samples were homogeneously diluted with silica. The mixtures were placed in a homemade cell equipped with quartz window. Steady-state photoluminescence spectra were recorded on a Jobin-Yvon Horiba Fluorolog FL-3-11 Tau 3 spectrofluorimeter using band pathways of 3 nm for both excitation and emission. Phosphorescence lifetimes were recorded with a Fluoromax phosphorimeter accessory containing a UV xenon flash tube with a flash rate between 0.05 and 25 Hz. Phase shift and modulation were recorded over the frequency range of 0.1−100 MHz. The lifetime data were fitted using the Jobin-Yvon software package and the Origin 6.0 and 7.5 program.

Synthesis of [Pd(bzq)(NCMe)$_2$]ClO$_4$ (1). $AgClO_4$ (0.712 g, 3.434 mmol) was added to a stirred suspension of **B** (0.110 g, 1.718 mmol) in MeCN (100 mL). After stirring at room temperature for 2 h in the dark, the mixture was filtered through Celite and the resulting solution evaporated to dryness. Addition of Et_2O (30 mL) to the residue gave pure **3** as a white solid. Yield: 0.151 g, 94%. Anal. Calcd for $C_{17}H_{14}ClN_3O_4Pd$: C, 43.79; H, 3.02; N, 9.01. Found: C, 43.29; H, 2.65; N, 8.70. MS (ES+): *m/z* 325 [Pd(bzq)(NCMe)]$^+$ 75%. IR (cm^{-1}): 2356 (m, NCMe), 2330 (m, sh, NCMe), 2305 (m, ν_{st}(C−N), NCMe); 1097 (vs, ν_3 ClO_4^-), 623 (s, ν_4 ClO_4^-). Λ_M (5×10^{-4} M acetonitrile solution): 122.6 Ω^{-1} cm^2 mol^{-1}.^{1}H NMR (400.13 MHz, CD_3CN, 298K, δ): 8.65 (s, H^2, bzq), 8.52 (d, $^3J_{H4-H3}$ = 7.9, H^4, bzq), 7.83 (AB, H^5, bzq), 7.75 (AB, $^3J_{H6-H5}$ = 8.6, H^6, bzq), 7.73 (d, $^3J_{H9-H8}$ = 7.3, H^9, bzq), 7.60 (dd, $^3J_{H3-H4}$ = 7.9, $^3J_{H3-H2}$ = 5.4, H^3, bzq), 7.44 (t, $^3J_{H8-H9/7}$ = 7.3, H^8, bzq), 7.36 (d, $^3J_{H7-H8}$ = 7.3, H^7, bzq), 1.99 (s, 6H, MeCN).

Synthesis of [Pd(ppy)(NCMe)$_2$]ClO$_4$ (2). This complex was prepared in the same way as **1**. $AgClO_4$ (0.700 g, 3.381 mmol), **D** (0.100 g, 1.688 mmol). **2**: white color. Yield: 0.142 g, 95%. Anal. Calcd for $C_{15}H_{14}ClN_3O_4Pd$: C, 40.74; H, 3.19; N, 9.50. Found: C, 40.42; H, 3.30; N, 9.73. IR (cm^{-1}): 2331 (m, NCMe), 2320 (m, NCMe), 2302 (m, ν_{st}(C−N), NCMe), 2291 (m, ν_{st}(C−N), NCMe); 1089 (s, ν_3 ClO_4^-), 624 (s, ν_4 ClO_4^-). Λ_M (5×10^{-4} M acetonitrile solution): 129.2 Ω^{-1} cm^2 mol^{-1}. ^{1}H NMR (400.13 MHz, CD_3CN, 298 K, δ): 8.43 (d, $^3J_{H2-H3}$ = 4.4, H^2, ppy), 8.04 (td, $^3J_{H4-H3}$ = $^3J_{H4-H5}$ = 8.1, $^4J_{H4-H2}$ = 1.2, H^4, ppy), 7.85 (d, $^3J_{H5-H4}$ = 8.1, H^5, ppy), 7.55 (dd, $^3J_{H6-H7}$ = 7.6, $^3J_{H6-H8}$ = 1.5, H^6, ppy), 7.32 (ddd, $^3J_{H3-H4}$ = 8.1, $^3J_{H3-H2}$ = 4.4, $^4J_{H3-H5}$ = 1.2, H^3, ppy), 7.25−7.10 (m, 3H, H^7, H^8, H^9, ppy), 1.99 (s, 6H, CH_3CN).

Synthesis of [Pt(bzq)(CN-*t*-Bu)$_2$]ClO$_4$ (5a). To a yellow suspension of [Pt(bzq)(NCMe)$_2$](ClO$_4$) (**3**) (0.200 g, 0.36 mmol) in methanol (15 mL) was added CN-*t*-Bu (83 μL, 0.72 mmol). After 2 h of stirring at room temperature, the solvent was evaporated to dryness, and the residue was treated with methanol (7 mL). The yellow solid was filtered and washed with Et_2O. Yield: 0.22 g, 95%. Anal. Calcd for $C_{23}H_{30}ClN_3O_4Pt$: C, 43.23; H, 4.10; N, 6.58. Found: C, 43.15; H, 3.80; N, 6.69. MS (ES+): *m/z* 539 [Pt(bzq)(CN-*t*-Bu)$_2$]$^+$ 100%. IR (cm^{-1}): 2235 (s, ν(C≡N)), 2210 (s, ν(C≡N)); 1097 (s, ν_3, ClO_4^-), 623 (s, ν_4, ClO_4^-). Λ_M (5×10^{-4} M nitromethane solution): 66.6 Ω^{-1} cm^2 mol^{-1}. ^{1}H NMR (400.13 MHz, CD_2Cl_2, 298 K, δ): 8.97 (dd, $^3J_{H2-H3}$ = 5.2, $^4J_{H2-H4}$ = 1.2, $^3J_{Pt-H2}$ = 34.5, H^2, bzq), 8.60 (dd, $^3J_{H4-H3}$ = 8.1, $^4J_{H4-H2}$ = 1.2, H^4, bzq), 7.82 (AB, $^3J_{H5-H6}$ = 8.7, H^5, bzq), 7.73 (m, H^3, H^9, bzq), 7.68 (dd, $^3J_{H7-H8}$ = 7.4, $^4J_{H7-H9}$ = 0.9, H^7, bzq), 7.65 (AB, $^3J_{H6-H5}$ = 8.7, H^6, bzq), 7.58 (t, $^3J_{H8-H9/7}$ = 7.4, H^8, bzq), 1.68 (s, 18H, CH_3, CN-*t-Bu*).

Synthesis of [Pt(bzq)(CN-*t*-Bu)$_2$]PF$_6$ (5b). To a yellow suspension of [{Pt(bzq)(μ-Cl)}$_2$] (**A**) (0.150 g, 0.183 mmol) in acetone (10 mL) were added CN-*t*-Bu (83 μL, 0.734 mmol) and $NaPF_6$ (0.062 g, 0.366 mmol). After 15 min of stirring at room temperature, the solvent was evaporated to dryness and the residue treated with CH_2Cl_2 (20 mL) and filtered through Celite. Evaporation of the filtrate to ca. 3 mL yielded **5b** as a yellow solid, which was filtered and washed with *n*-hexane. Yield: 0.174 g, 70%. Anal. Calcd for $C_{23}H_{26}F_6N_3PPt$: C, 40.36; H, 3.83; N, 6.14. Found: C, 40.38; H, 3.73; N, 6.54. MS (ES+): *m/z* 539 [Pt(bzq)(CN-*t*-Bu)$_2$]$^+$, 100%. IR (cm^{-1}): 2236 (s, ν(C≡N)), 2210 (s, ν(C≡N)). Λ_M (5×10^{-4} M acetonitrile solution): 160.9 Ω^{-1} cm^2 mol^{-1}. ^{1}H NMR (400.13 MHz, CD_2Cl_2, 298 K, δ): 8.81 (d, $^3J_{H2-H3}$ = 5.2, $^3J_{Pt-H2}$ = 34.5, H^2, bzq), 8.48 (d, $^3J_{H3-H4}$ = 8.1, H^4, bzq), 7.79 (AB, $^3J_{H5-H6}$ = 8.7, H^5, bzq), 7.70 (m, H^3, H^9, H^7, bzq), 7.65 (AB, $^3J_{H6-H5}$ = 8.7, H^6, bzq), 7.57 (t, $^3J_{H8-H9/7}$ = 7.6, H^8, bzq), 1.69 (s, 9H, CN-*t*-Bu), 1.68 (s, 9H, CN-*t*-Bu). ^{19}F NMR (282.40 MHz, CD_2Cl_2, 298 K, δ): −73.62 (d, J_{P-F} = 711, PF_6). ^{31}P{^{1}H} NMR (121.50 MHz, CD_2Cl_2, 298 K, δ): −142.5 (sept, J_{P-F} = 711, PF_6). ^{13}C{^{1}H} NMR (CD_2Cl_2, 75.50 MHz, 298 K, δ): 157.55 (s, C^{10}), 153.15 (s, $^2J_{Pt-C}$ = 31.6, C^2), 149.47 (s, C$^{13/14}$), 143.89 (s, C$^{13/14}$), 142.22 (s, C^4), 136.10 (s, $^2J_{Pt-C}$ = 104, C^9), 135.86 (s, $^3J_{Pt-C}$ = 48.1, C$^{11/12}$), 132.21 (s, $^3J_{Pt-C}$ = 64.5, C^8), 131.74 (s, C^5), 129.37 (s, $^3J_{Pt-C}$ = 34.3, C$^{11/12}$), 126.84 (s, C^7), 125.51 (s, C^6), 125.08 (s, C^3), 31.48 (s, *C*H$_3$, CN-*t*-Bu), 31.33 (s, *C*H$_3$, CN-*t*-Bu). ^{195}Pt NMR (86.02 MHz, CD_2Cl_2, 298 K, δ): −4246 (s br).

Synthesis of [Pt(bzq)(CN-Xyl)$_2$]ClO$_4$ (6a). Complex **6a** was prepared as a yellow solid according to a similar procedure to that for compound **5a** starting from [Pt(bzq)(NCMe)$_2$](ClO$_4$) (**3**) (0.191 g, 0.34 mmol) and CN-Xyl (0.092 g, 0.69 mmol). Yield: 0.232 g, 92%. Anal. Calcd for $C_{31}H_{26}ClN_3O_4Pt$: C, 50.65; H, 3.57; N, 5.72. Found: C, 50.91; H, 3.32; N, 5.70. MS (ES+): *m/z* 635.2 [Pt(bzq)(CN-Xyl)$_2$]$^+$, 100%. IR (cm^{-1}): 2204 (s, ν(C≡N)), 2184 (s, ν(C≡N)); 1087 (s, ν_3, ClO_4^-), 623 (s, ν_4, ClO_4^-). Λ_M (5×10^{-4} M nitromethane solution): 69.8 Ω^{-1} cm^2 mol^{-1}. ^{1}H NMR (400.13

(92) Pregosin, P. S.; Wombacher, F.; Albinati, A.; Lianza, F. *J. Organomet. Chem.* **1991**, *418*, 249.
(93) Hartwell, G. E.; Lawrence, R. V.; Smas, M. J. *Chem. Commun.* **1970**, 912.
(94) Craig, C. A.; Watts, R. J. *Inorg. Chem.* **1989**, *28*, 309.

Table 5. Crystal data and structure refinement parameters for complexes 6a·CH_2Cl_2 and 6b·CH_2Cl_2

	6a·CH_2Cl_2	6b·CH_2Cl_2
empirical formula	$C_{32}H_{28}Cl_3N_3O_4Pt$	$C_{32}H_{28}Cl_2F_6N_3PPt$
fw	820.01	865.53
temperature (K)	100(2)	100(2)
wavelength (Å)	0.71073	0.71073
cryst syst	monoclinic	monoclinic
space group	*P*2(1)/*n*	*P*1 21/*n* 1
cryst dimens (mm)	0.41 × 0.27 × 0.21	0.32 × 0.14 × 0.12
a (Å)	16.0067(2)	8.28410(10)
b (Å)	10.8311(2)	17.3713(2)
c (Å)	18.2324(3)	21.6571(2)
α (deg)	90	90
β (deg)	106.363(2)	90.8380(10)
γ (deg)	90	90
V (Å^3)	3032.92(8)	3116.24(6)
D_{calc} (Mg/m^3)	1.796	1.845
Z value	4	4
μ(Mo Kα) (mm^{-1})	4.934	4.790
F(000)	1608	1688
θ range (deg)	3.82 to 25.10	3.77 to 25.10
no. of reflns measd	20 262	20 635
no. of obsd reflns	5383	5517
goodness of fit on F^{2a}	1.068	1.020
final *R* indices [$I > 2\sigma(I)$]^a	$R_1 = 0.0167$, $wR_2 = 0.0403$	$R_1 = 0.0147$, $wR_2 = 0.0375$
R indices (all data)	$R_1 = 0.0198$, $wR_2 = 0.0170$	$R_1 = 0.0170$, $wR_2 = 0.0381$

^{a} $R_1 = \sum(|F_o| - |F_c|)/\sum|F_o|$; $wR_2 = [\sum w(F_o^2 - F_c^2)^2/\sum wF_o^2]^{1/2}$; Goodness of fit = $\{\sum[w(F_o^2 - F_c^2)^2]/(N_{obs} - N_{param})\}^{1/2}$; $w = [\sigma^2(F_o^2) + (g_1P)^2 + g_2P]^{-1}$; $P = [\max(F_o^2;0) + 2F_c^2]/3$.

MHz, CD_2Cl_2, 298 K, *δ*): 9.14 (dd, $^3J_{H2-H3} = 5.3$, $^4J_{H2-H4} = 1.0$, $^3J_{Pt-H2} = 37.8$, H^2, bzq), 8.61 (d, $^3J_{H4-H3} = 8.1$, H^4, bzq), 7.91 (d, $^3J_{H9-H8} = 7.6$, $^3J_{Pt-H9} = 48.7$, H^9, bzq), 7.89 (AB, $^3J_{H5-H6} = 8.7$, H^5, bzq), 7.79 (d,$^3J_{H7-H8} = 7.6$, H^7, bzq), 7.75 (dd, $^3J_{H3-H4} = 8.1$, $^3J_{H3-H2} = 5.3$, H^3, bzq), 7.72 (AB, $^3J_{H6-H5} = 8.7$, H^6, bzq), 7.60 (t, $^3J_{H8-H9/7} = 7.6$, H^8, bzq), 7.36−7.23 (AB_2, 2H^4, 2H^3, 2H^5, Xyl), 2.53 (s, 12H, C*H*$_3$-Xyl).

Synthesis of [Pt(bzq)(CN-Xyl)$_2$]PF_6 (6b). Complex **6b** was prepared as a yellow solid according to a similar procedure to that for compound **5b** starting from [{Pt(bzq)(*μ*-Cl)}$_2$] (**A**) (0.100 g, 0.122 mmol), CN-Xyl (0.064 g, 0.488 mmol), and $NaPF_6$ (0.041 g, 0.244 mmol). Yield: 0.145 g, 76%. Anal. Calcd for $C_{31}H_{26}F_6N_3PPt$: C, 47.70; H, 3.36; N, 5.38. Found: C, 47.64; H, 3.12; N, 5.74. MS (ES+): *m*/*z* 635.4 [Pt(bzq)(CN-Xyl)$_2$]$^+$, 100%. IR (cm^{-1}): 2208 (s, *ν*(C≡N)), 2187 (s, *ν*(C≡N)). Λ_M (5×10^{-4} M acetonitrile solution): 164.7 Ω^{-1} cm^2 mol^{-1}.^{1}H NMR (400.13 MHz, CD_2Cl_2, 298 K, *δ*): 9.24 (d, $^3J_{H2-H3} = 5.2$, $^3J_{Pt-H2} = 37.8$, H^2, bzq), 8.71 (d, $^3J_{H4-H3} = 8.1$, H^4, bzq), 8.02 (d, $^3J_{H9-H8} = 7.6$, $^3J_{Pt-H9} = 48.3$, H^9, bzq), 7.98 (AB, $^3J_{H5-H6} = 9.0$, H^5, bzq), 7.91 (d, $^3J_{H7-H8} = 8.0$, H^7, bzq), 7.83 (AB, $^3J_{H5-H6} = 9.0$, H^6, bzq + H^3 overlapped), 7.72 (t, $^3J_{H8-H9/7} = 7.7$, H^8, bzq), 7.52−7.33 (AB_2, 2H^4, 2H^3, 2H^5, Xyl), 2.64 (s, 12H, C*H*$_3$-Xyl). ^{19}F NMR (282.40 MHz, CD_2Cl_2, 298 K, *δ*): −72.59 (d, $J_{P-F} = 711$, PF_6). ^{31}P{^{1}H} NMR (121.50 MHz, CD_2Cl_2, 298 K, *δ*): −142.5 (sept, $J_{P-F} = 711$, PF_6). ^{13}C{^{1}H} NMR (75.50 MHz, CD_2Cl_2, 298 K, *δ*): 157.80 (s, C10), 153.37 (s, $^2J_{Pt-C} = 31.2$, C^2), 149.83 (s, C$^{13/14}$), 148.08 (s, C$^{13/14}$), 142.88 (s, C^4), 137.81 (s, 2C$_o$, Xyl), 137.55 (s, C$^{11/12}$), 136.94 (s, C^9), 136.23 (s, 2C$_o$, Xyl), 133.08 (s, C$_p$, Xyl), 132.70 (s, C$_p$, Xyl), 132.49 (s, C^8), 132.06 (s, C^5), 130.35 (s, C$_m$, Xyl), 130.30 (s, C$_m$, Xyl), 129.78 (s, C$^{11/12}$), 127.46 (s, C^7), 125.71 (s, C^3), 125.55 (s, C$_{ipso}$, Xyl), 125.20 (s, C^6), 120.77 (s, C$_{ipso}$, Xyl), 20.36 (s, 2*C*H$_3$, Xyl), 20.31 (s, 2*C*H$_3$, Xyl). ^{195}Pt NMR (86.02 MHz, CD_2Cl_2, 298 K, *δ*): −4168 (s br).

Synthesis of [Pt(bzq)(CN-2-Np)$_2$]ClO_4 (7a). Complex **7a** was prepared as a yellow solid according to a similar procedure to that for compound **5a** starting from [Pt(bzq)(NCMe)$_2$](ClO_4), **3** (0.161 g, 0.29 mmol), and CN-2-Np (0.089 g, 0.58 mmol). Yield: 0.203 g, 90%. Anal. Calcd for $C_{35}H_{22}ClN_3O_4Pt$: C, 53.96; H, 2.85; N, 5.39. Found: C, 53.72; H, 2.80; N, 5.27. MS (ES+): *m*/*z* 679.2 [Pt(bzq)(CN-2-Np)$_2$]$^+$, 100%. IR (cm^{-1}): 2217 (s, *ν*(C≡N)), 2190 (s, *ν*(C≡N)); 1093 (s, ν_3, ClO_4^-), 623 (s, ν_4, ClO_4^-). Λ_M (5×10^{-4} M nitromethane solution): 65.5 Ω^{-1} cm^2 mol^{-1}. ^{1}H NMR (400.13 MHz, CD_3CN, 298 K, *δ*): 8.67 (d, $^3J_{H2-H3} = 5.1$, $^3J_{Pt-H2} = 35$, H^2, bzq), 8.29 (d, $^3J_{H4-H3} = 7.9$, H^4, bzq), 8.24 (s, H^1, Np), 8.16 (s, H$^{1'}$, Np), 7.84 (m, 7H, Np/bzq), 7.61 (m, 9H, Np/bzq), 7.47 (d, *J* = 8.5, 1H, bzq), 7.41 (dd, $^3J_{H3-H4} = 7.9$, $^3J_{H3-H2} = 5.1$, H^3, bzq).

Synthesis of [Pt(bzq)(CN-2-Np)$_2$]PF_6 (7b). A yellow suspension of [{Pt(bzq)(*μ*-Cl)}$_2$] (**A**) (0.100 g, 0.122 mmol) in acetone (10 mL) was treated with CN-2-Np (0.075 g, 0.488 mmol) and $NaPF_6$ (0.040 g, 0.245 mmol), giving an initial red suspension. The mixture was stirred for 15 min, changing the color to a yellow suspension. The solvent was removed and the final residue was treated with water (20 mL) and filtered. Yield: 0.176 g, 87%. Anal. Calcd for $C_{35}H_{22}F_6N_3PPt$: C, 50.98; H, 2.69; N, 5.10. Found: C, 51.40; H, 2.89; N, 5.04. MS (ES+): *m*/*z* 678.8 [Pt(bzq)(CN-2-Np)$_2$]$^+$, 100%. IR (cm^{-1}): 2215 (s, *ν*(C≡N)), 2189 (s, *ν*(C≡N)). Λ_M (5×10^{-4} M acetonitrile solution): 137.7 Ω^{-1} cm^2 mol^{-1}. ^{1}H NMR (300.13 MHz, CD_3CN, 298 K, *δ*): 8.52 (d, $^3J_{H2-H3} = 4.8$, $^3J_{Pt-H2} = 35$, H^2, bzq), 8.21 (d, $^3J_{H4-H3} = 7.9$, H^4, bzq), 8.16 (s, H^1, Np), 8.08 (s, H$^{1'}$, Np), 7.82 (m, 6H, Np/bzq), 7.60 (m, 10H, Np/bzq), 7.40 (d, *J* = 8.5, 1H, bzq), 7.30 (dd, $^3J_{H3-H4} = 7.6$, $^3J_{H3-H2} = 5.4$, H^3, bzq). The low solubility of this complex precludes its characterization by ^{13}C{^{1}H} and ^{195}Pt NMR.

Computational Details. The computational method used was density functional theory (DFT) with the B3LYP exchange−correlation functional,[95−97] using the Gaussian 03[98] program package. The basic set used was the LanL2DZ effective core potential for the platinum atom and 6-31G(d,p) for the remaining atoms. Cation **6**$^+$ was optimized as an isolated molecule from the solid-state geometry at the DFT level of theory. The time-dependent density-functional theory (TD-DFT) calculation was carried out using the polarized continuum model approach implemented in the Gaussian 03 software.

X-ray Structure Analysis of 6a·CH_2Cl_2 and 6b·CH_2Cl_2. Crystal data and other details of the structure analyses are presented in Table 5. Yellow needles were obtained by slow diffusion of *n*-hexane (**6a**) or 2-propanol (**6b**) into dichloromethane (at 5 °C) solutions of each compound. Single crystals were mounted in quartz fibers in a random orientation and held in place with fluorinated oil. Data collections were performed at 100 K temperature on an Oxford Diffraction Xcalibur CCD diffractometer using graphite-monochromated Mo Kα radiation ($\lambda = 0.71073$ Å) with a nominal crystal to detector distance of 5.0 cm. Unit cell dimensions were determined from the positions of 16 979 reflections from the main data set for 6a·CH_2Cl_2 and from the positions of 18 152 reflections from the main data set for 6b·CH_2Cl_2. Sets of data were collected for the two structures based on *ω*-scans runs. The diffraction frames were integrated and corrected for absorption using the Crysalis RED package.[99] Lorentz and polarization corrections were applied. The structures were solved by direct methods. All non-hydrogen atoms were assigned anisotropic displacement parameters. The hydrogen atoms were constrained to idealized geometries and assigned isotropic displacement parameters equal to 1.2 times the U_{iso} values of their respective parent carbon toms (1.5 times for methyl H atoms). Full-matrix least-squares refinement of these models against F^2 using the SHELXL-97 program[100] converged to final residual

(95) Becke, A. D. *Phys. Rev. A: At., Mol., Opt. Phys.* **1988**, *38*, 3098.
(96) Lee, C.; Yang, W.; Parr, R. G. *Phys. Rev. B: Condens. Matter Mater. Phys.* **1988**, *37*, 785.
(97) Becke, A. D. *J. Chem. Phys.* **1993**, *98*, 5648.
(98) Frisch, M. J.; et al. *Gaussian 03, Revision E.01*; Gaussian, Inc.: Wallingford, CT, 2004 (see Supporting Information for complete citation).
(99) *CrysAlis; RED. A program for Xcalibur CCD System X-ray diffraction data reduction*; Oxford Diffraction Ltd.: Oxford, UK, 2005.

indices given in Table 5. Final difference electron density maps showed no peaks above 1 e $Å^{-3}$ for both structures.

Acknowledgment. This work was supported by the Spanish Ministerio de Educación y Ciencia and FEDER funds (Projects CTQ2008-06669-C02-01,02/BQU and CTQ2005-06807/BQU and a grant for A.D.).

Supporting Information Available: Drawing, table of atomic coordinates, and excitation calculations for the DFT-optimized structure of cation $\mathbf{6}^+$ and representative frontier orbitals for it (Tables S1 and S2 and Figures S3 and S4). Table S3: Emission data for complexes **5**−**7** in other solvents (5×10^{-5} M solutions at 298 K). Absorption spectra (Figures S1, S2, S5, S6). Emission spectra (Figures S7−S16). Crystallographic data in CIF format. This material is available free of charge via the Internet at http://pubs.acs.org.

OM800845C

(100) Sheldrick, G. M. *SHELXL-97, a program for crystal structure determination*; University of Göttingen: Göttingen, Germany, 1997.